Clemens Konstantin Stilianu, B.Sc.

Experimental Setup for Laser Induced Single Cell Electrophysiological Recordings with Organic Semiconductors

MASTER'S THESIS

to achieve the university degree of
Diplom-Ingenieur

Master's degree programme:
Technical Physics

submitted to
Graz University of Technology

Supervisor

Assoz. Prof. Dipl.-Ing. Dr.techn. Georg Pabst
Institute of Materials Physics

Co-Supervisor
Univ.-Ass. Priv.-Doz. Dipl.-Ing. Dr.techn. Rainer Schindl
Institute of Biophysics Medical University of Graz

Graz, August 2020

AFFIDAVIT

I declare that I have authored this thesis independently, that I have not used other than the declared sources/resources, and that I have explicitly indicated all material which has been quoted either literally or by content from the sources used. The text document uploaded to TUGRAZonline is identical to the present master's thesis.

31.08.2020 

Date, Signature

Acknowledgements

I would like to thank Prof. Georg Pabst for the good collaboration during the process of this thesis. With deep gratitude I would like to thank Rainer Schindl, PhD for giving me the opportunity to join his team to work on this interesting masters thesis. With his extraordinary support and an ongoing constructive and lively exchange he took a big part in the results of this thesis.

To get into the field of biophysics as technical physicist I needed to catch up on basic principles of biology and biochemistry, therefore I would like to thank my colleague Tony Schmidt on the one hand for teaching me various concepts of life science and on the other hand for the collaboration on this project and for taking a big part in the experimental results.

I would also like to thank my physics colleagues at the Graz University of Technology for being a great and supportive community.

Furthermore I want to thank my sister Teresa Stilianu for all the productive conversations about life science and I want to thank my mother Dr. Gabriele Stilianu for always supporting me with her knowledge of physiology and medicine.

Last but not least I want to thank my girlfriend Helene Windhaber for her tremendous support and for keeping me sane.

Contents

1. Abstract

Light control of organism and cells is a favourable method for non-invasive stimulation. Optoelectronic devices can directly generate electrical signals upon a light pulse in attached excitable cells by depolarizing the membrane potential and fire action potentials. Organic semiconductors suggest being a promising material in respect of optical and electrical properties as well as non-toxicity and bio-compatibility. In this thesis I will introduce an experimental method to generate cell membrane depolarisation by focusing a laser light beam onto 3D shaped epindolidione organic semiconductor pigments. In live cell experiments, the change in the cell membrane potential is measured with the patch-clamp technique at the same time. This electrophysiological technique clamps a single cell to record membrane currents or membrane potentials in real-time. A short ms laser pulse allows to directly transfer light induced depolarisation to the cell membrane via a rapid change in membrane capacity in order to efficiently generate an depolarizing current within the cell. Here, I use organic pigments that are shaped in 3D structures and are few μm in size to form a perfect interface with the plasma membrane of living cells. To ensure easy focusing of the beam, while conducting patch-clamp recordings, the laser beam is directly coupled into an inverted microscope. The first proof of concept experiments with this setup exhibit a small but significant change in the cell membrane potential. Current laser pulses with a minimal length of 10 ms are expected to rapidly change the membrane potential via the photo induced thermocapacitive effect. Further experiments are discussed to optimize cell stimulation with considerably shorter μs-range and more intense laser pulses and thus ultimately trigger action potentials in neuronal cells. In conclusion, my experiments demonstrate that 3D shaped bio-compatible organic semiconductor epindolidione pigments can be used to depolarize attached cells with a short laser light pulse.

2. Introduction

2.1. Artificial stimulation of living cells with organic semiconductors

The pigment quinacridone has been successfully used as light-regulated semiconductor. Quinacridone, shaped as nano-crystals (also called hedgehog structures) can be used to efficiently interact with living cells [15]. The geometry of the organic semiconductor pigment results in an extremely small gap as well as a very large contact surface between the cell membrane and the organic semiconductor. This gives optimal conditions to stimulate cells by changing the membrane potential.

By focusing (laser) light pulses onto the pigments it is possible to rapidly change the membrane temperature and therefore change the membrane capacitance, which ultimately results in cell stimulation [3] (this concept is discussed later in detail in section 3.2).

2.2. Aim and approach

The objective of this master thesis is to construct an experimental setup which is capable of changing the cell membrane potential of living cells in contact with organic semiconductor pigments using laser light. By coupling a laser into an inverted microscope it is possible to focus the laser light pulses directly onto the semiconductor structures, while making electrophysiological recordings (patch clamp recordings) feasible. The setup mainly consists of a microscope, a custom built laser unit, electrophysiological measuring equipment and a programmable laser controlling circuit. An important advantage of this laser-electrophysiological microscope is the low cost laser adjustment that easily allows

to substitute for various wavelengths.

To proof that the concept of laser induced single cell stimulation with organic semiconductors is possible with this setup, the first measurements are included in this thesis as well as suggestions for further improvements.

2.3. Possible applications for light induced cell stimulation with organic semiconductor pigments

A physiological application is to stimulate neurons in the human retina when photoreceptor cells [1] are degenerated. For example a well-known inherited disorder called "retinitis pigmentosa" leads to a degeneration of the photoreceptive cells in the retina while the neurons responsible for the nervous conduction of the stimuli are still working. An injection of organic semiconductor pigments into the retina, specifically in close contact to the retinal ganglion cells, may be an option to reverse the effects of the retina degeneration [15] (see fig. 1).

A second possible application is the regeneration of neuronal networks after a traumatic stroke that is currently investigated by LOGOS-TBI team headed by Muammer Ücal, PhD at the Medical University of Graz.

[1] Photoreceptor cells in the retina of the mammalian eye, also called rod and cone cells, are responsible for ganglion (neuron) stimulation through light absorption [11]

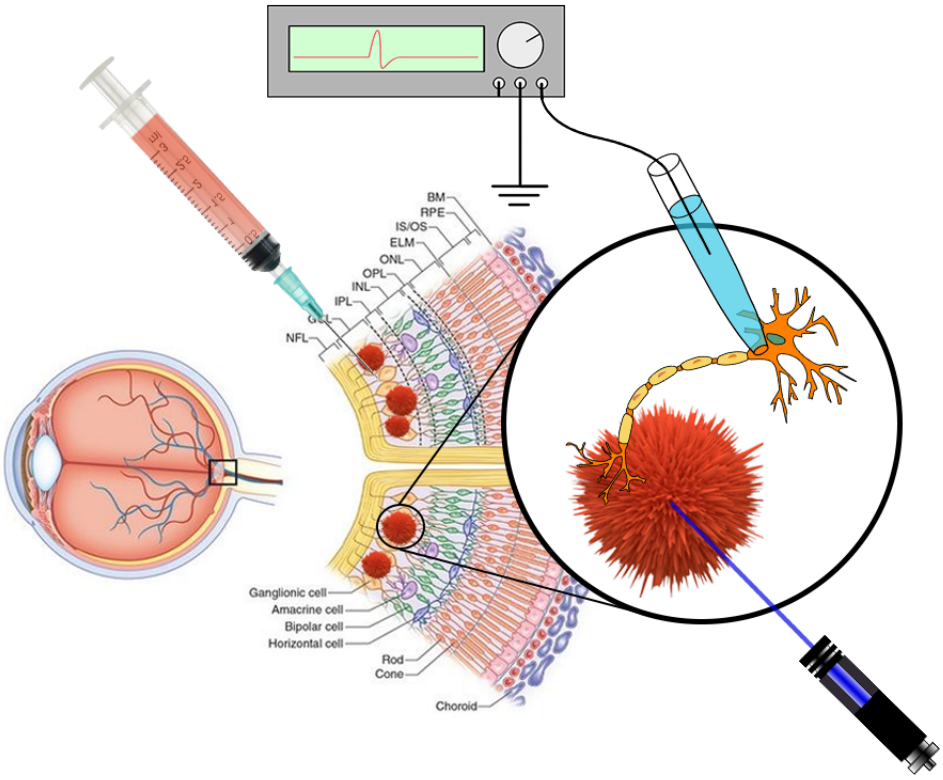

Figure 1: A possible application for light induced cell stimulation with organic semiconductor pigments might be the treatment of degenerative diseases concerning the retina of the human eye. In this figure the basic principle of artificial neuron stimulation with organic semiconductor injections into the eye is shown. Semiconductor pigments absorb light to generate a stimulus in the connected neurons. The inset depicts how neuronal signals can be recorded in real time using the patch clamp technique.

3. Theoretical principals

3.1. Basic concepts of electrophysiology

In order to address a living cell, for example a neuron, it is crucial to understand the basic concepts of electrophysiology. Every living cell is surrounded by a plasma membrane which separates the interior of the cell from its outside. In the simplest case the plasma membrane is formed of a phospholipid bilayer. This membrane is in general not permeable for polar molecules and charged atoms, such as dissolved salt components like Na^+, K^+, Cl^- and Ca^{2+}.

For a physiological (natural and healthy) environment certain concentrations of ions inside the cell need to be maintained. The flow of ions through this non-permeable membrane is controlled via proteins, the so called ion channels. These ion channels are mainly selective for either Na^+, K^+, Cl^- and Ca^{2+} ions. (see fig. 2) [9, p.1-5].

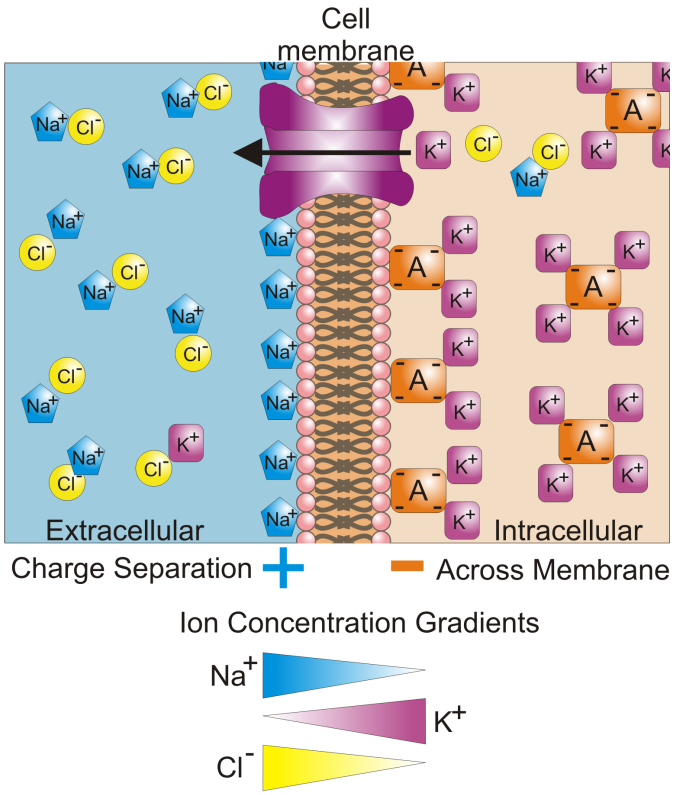

Figure 2: Charge separation between the intracellular and extracellular medium (concentration gradients) of important ions enabled trough selective ion pumps. [21]

Therefore having different ion concentrations leads to ion concentration gradients and a charge separation. This charge separation is then generating an electrical field where the potential can be described via the Nernst potential,

$$V_k = \frac{RT}{q_k F}\, ln \frac{[C_k]_o}{[C_k]_i}, \tag{1}$$

where V_k is the electrical potential created by the separated ions of the species k, their charge q_k, R the gas constant, F the Faraday's constant, $[C_k]_o$ the concentration C of the species k outside of the plasma membrane and $[C_k]_i$ the concentration C of the species k inside of the plasma membrane.

With the superposition principle one can combinde the potentials to the netto membrane potential,

$$V_M = \frac{RT}{F} \sum_{k=1}^{N=4} \frac{1}{q_k} \, ln\frac{[C_k]_o}{[C_k]_i} = \frac{RT}{F} \left(ln\frac{[Na]_o}{[Na]_i} + ln\frac{[K]_o}{[K]_i} + 2ln\frac{[Ca]_o}{[Ca]_i} - ln\frac{[Cl]_i}{[Cl]_o} \right). \quad (2)$$

The sign of the terms origins on the one hand from the different signs of the charges and on the other hand from the definition that the membrane potential is measured from inside minus outside. In a typical mammalian cell this resting membrane potential adds up to around $V_{M0} = -40\ mV$ to $V_{M0} = -95\ mV$ [9, p.13-17].

3.1.1. The cell as capacitor

The phospholipid bilayer which forms the plasma membrane separates internal and external conducting solutions by an very thin (minimum $3-4\ nm$) insulating layer. As the conducting solution inside the cell is completely surrounded by this insulating layer this structure can be treated as a spherical capacitor with significant capacitance. However the different kinds of ion channels can be opened and closed under several conditions. In respect to the electrical behaviour the voltage dependent gating mechanisms play an important role. Therefore the plasma membrane can be seen as electrical resistor with a time and voltage dependent part [2] $R_M(t) = R_{const} + R(V(t))$. The electrical equivalent circuit in fig. 3 shows a simplification of this electrical behaviour. This circuit also includes the resting membrane potential V_{M0} (see eq. (2)) as an additional voltage source to set the zero reference point of the cell membrane potential to a negative potential [9, p.10-12].

[2] The membrane is of course not a perfect insulator, proteins and other biological mechanisms lead to a constant leakage of charges.

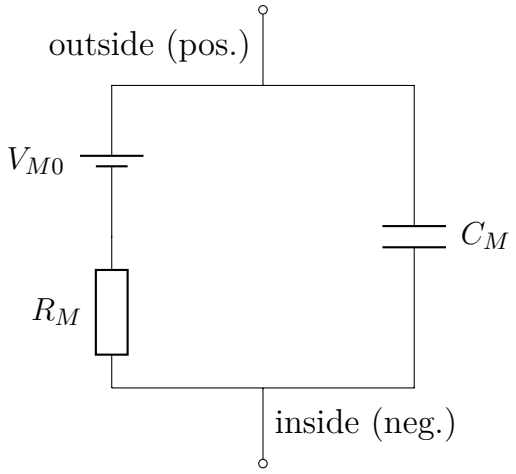

Figure 3: Electrical equivalent circuit of the cell depicting the electrical behaviour of the cell plasma membrane and the ion channels. V_M is the resting potential. R_M the resistance of the membrane with the channels and C_M is the capacitance formed by the cell geometry. [9]

It is also important to mention that in this models we are always talking about physical current direction, where the electrical field and the potentials are defined in a way that the positive ions move from the positive pole (outside the cell membrane) to the negative pole (inside the cell membrane).

To estimate the electrical capacitance of a living cell one needs to observe the electrical behaviour in a dynamic circuit. We start with the definition of a capacitor,

$$C_M = \frac{Q_M(t)}{V(t)}, \tag{3}$$

with Q_M beeing the charges held by the capacitor (membrane) and $V(t)$ the voltage measured from the interior to the exterior of the cell. The rate of change can be expressed by the time derivative of equation 3:

$$\frac{dV(t)}{dt} = \frac{I_C(t)}{C_M}, \tag{4}$$

where $I_C = {}^{dQ_M(t)}/_{dt}$ is the capacitive current through the cell membrane. The capacitance of the plasma membrane is of course a function of the dielectric function ε and the geometry of the capacitor G:

$$C_M \propto \varepsilon(T)G(A,d). \tag{5}$$

The geometry mainly depends on the thickness d and the Area A. T is the Temperature of the cell membrane. The significant capacitance of roughly 1.0 ${}^{F}/_{cm^2}$ ($= 0.1$ ${}^{pF}/_{m^2}$) of the plasma membrane origins from the relatively high dielectric constant of lipids and carbon. This means one can calculate the approximate thickness of the membrane to around $d \approx 23$ $\mathring{A}$ (assuming a parallel-plate capacitor $C_m = {}^{\varepsilon\varepsilon_0 A}/_{d}$) [2, 5].

A simple way to measure the capacitance is to look at the step response of the membrane potential $V_M(t)$ when a rectangular voltage is applied to the cell. A capacitor discharges through a resistor over time as shown in equation (4). With Ohm's law this equation becomes:

$$\dot{V} = \frac{dV(t)}{dt} = \frac{I_C(t)}{C_M} = -\frac{V(t)}{R_M C_M}. \tag{6}$$

This ordinary first-order differential equation has the solution

$$V = V_0 \; exp\left(-\frac{t}{R_M C_M}\right) = V_0 \; exp\left(-\frac{t}{\tau_M}\right), \tag{7}$$

where V_0 is the starting voltage and $\tau_M = R_M C_M$ is the membrane time constant. After the time τ_M the membrane potential is at $exp(-\frac{t=\tau_M}{\tau_M}) = 1/e \approx 37$ % of its maximum value V_0. [9, p.10-12]

3.1.2. The patch-clamp technique

A convenient method to measure electrical properties of a single living cell is the patch-clamp technique. The idea is to record electrical dynamics from a tiny area ("patch") of surface membrane by attaching a glass pipette to a living cell. The interior of the glass pipette is usually filled with an electrolyte that is in contact with a silver chloride electrode ($Ag/AgCl$). Using an amplifier and a reference electrode in the same solution forms a closed circuit where electrical measurements are feasible (see fig. 4). On one hand it is possible to measure the ion current $I_M(t)$ through the membrane by holding the voltage constant $V_M = const$, also called "voltage clamp" mode, on the other hand it is possible to measure the membrane potential $V_M(t)$ while holding the ion current constant $I_M = const$, also called "current clamp".

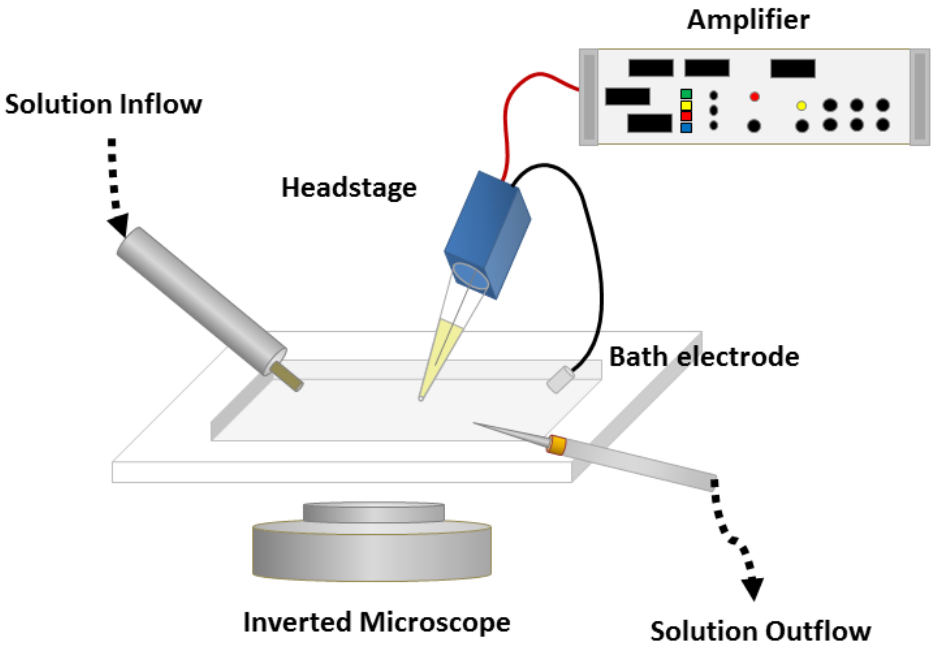

Figure 4: Typical patch clamp setup for electrophysiological recordings. The glass pipette is usually connected to a headstage pre amplifier and a patch clamp amplifier. The circuit is closed with the reference bath electrode in the same electrolyte. In this figure there is also solution in- and outflow to change ion concentrations in the sample electrolyte. [20]

Clean glass pipettes can fuse with the plasma membrane of the cell forming a seal with very high electrical resistance. This seal is called a "gigaseal" since the recorded electrical resistance is in the order of gigaohms $R_M = 10^9\ \Omega$. The gigaseal permitts four different electrical recording configurations (see fig. 5). Firstly one can record ion currents through single ion channels with the "on-cell" or "cell-attached" method in voltage clamp mode. Secondly one can apply suction to the membrane by reducing the pressure inside the pipette . This seal is then mechanically stable enough to be pulled off the cell and still seal the pipette - the "inside-out" or "excised-patch" configuration. Thirdly an on-cell attachment can be used to rupture the cell membrane by applying additional suction. This is called the "whole-cell" configuration, which allows to integrate

the whole cell with its interior as an electrical component into the circuit. The fourth, the "outside-out" configuration, is achieved by pulling the pipette away from the whole-cell configuration. [9, p.87-88]

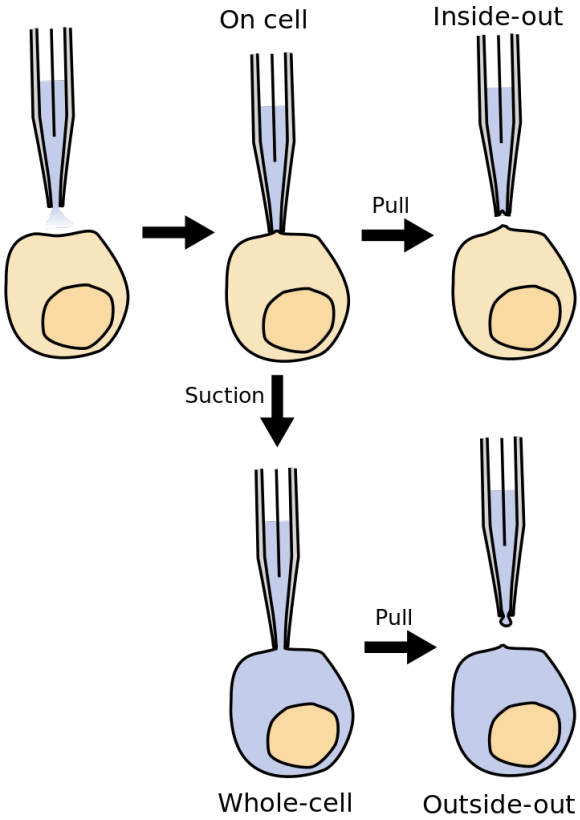

Figure 5: The four gigaseal configurations for patch clamp recordings. With this methods it is either possible to measure ion current $I_M(t)$ or the membrane potential $V_M(t)$ with voltage clamp or current clamp. This can be done either for small parts of the membrane (even single ion channels) or for the whole cell. [18]

3.1.3. Basic principle of cell stimulation and action potential with the patch clamp technique

By using electrophysiological recording methods like patch clamp it is possible to rupture the plasma membrane and integrate a whole cell into an electrical circuit. The patch clamp amplifier is zeroed with the pipette outside of the cell. Just as the pipette is fused with the cell a negative potential can be mea-

sured. This is the resting membrane potential V_{M0} from equation (2) resulting from the Nernst potential equation (1). By using the current clamp mode the ionic current through the cell membrane is held constant $I_M = const.$ Clamping the current to zero $I_M = 0$ results in the membrane potential to be the resting potential $V_M(t) = V_{M0}$. Increasing the current therefore leads to a membrane potential which is higher than the resting membrane potential $V_M > V_{M0}$. This mechanism is called cell membrane depolarization. After the cell membrane potential exceeds some threshold potential this leads to a phenomenon called the "action potential". This phenomenon only occurs in excitable cells (neurons, muscle cells and some endocrine cells).

When the membrane potential exceeds the threshold potential, voltage gated ion channels open up resulting in further depolarization (see fig. 6). [6, p.44-46] [9, p.25-42] The proteins responsible for this depolarization are voltage gated sodium and potassium channels. Sodium channels depolarize the membrane, while potassium channels recover the resting potential. The sodium channels open up faster than the potassium channels resulting in a rapid rise of sodium conductivity $g_{Na}(t)$ and depolarization of the membrane potential (see fig. 7). This effect can add up to a peak membrane potential of roughly $V_M = +20\ mV$ to $V_M = +30\ mV$. After approximately 1 ms [3] the sodium conductivity goes to zero again while the conductivity of potassium ions $g_K(t)$ rises, this results in a repolarization of the membrane potential. Note that the charge of the sodium Na^+ and potassium K^+ ions are both positive but the concentration gradients are opposite. [6, p.46]

[3] 1 ms for neuronal cells. In heart cells this much slower.

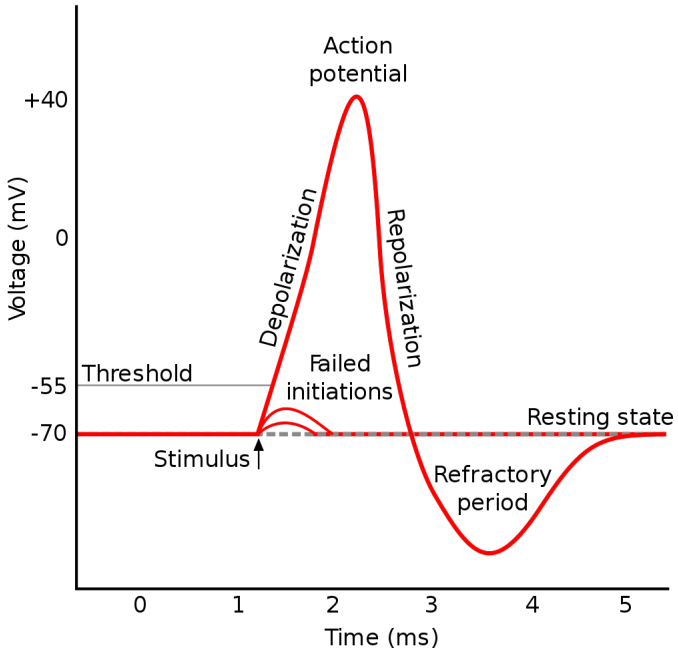

Figure 6: Principle of generating an action potential by depolarization of a cell membrane. After reaching the threshold voltage, voltage dependent ion channels are responsible for fast de- and repolarization of the cell membrane. [19]

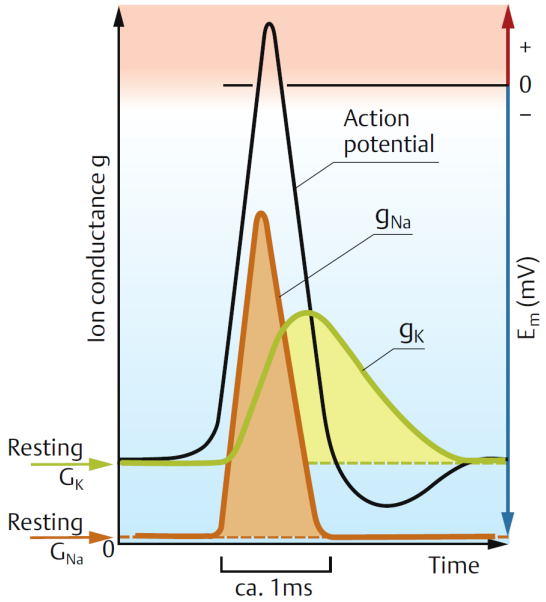

Figure 7: The conductance of voltage gated sodium channels $g_{Na}(t)$ and potassium channels $g_K(t)$ add up to the action potential. G_{Na} and G_K are the resting ion conductivity. [6, p.47]

3.1.4. Different ways of cell stimulation

There are different effects that can lead to membrane depolarization of living cells and therefore to action potential generation. Mainly there are three important effects which dominate artificial cell stimulation:

- Capacitive effect

The capacitive effect is caused by a charge carrier separation that induces a potential difference $\Delta V = q/C$ between the interior and exterior of the cell (see section 3.1.1). By locating an external potential near a living cell it is possible to depolarize a cell membrane to the point of generating an action potential. This effect is one of the basic principles of the patch clamp technique (see section 3.1.2). This effect is also seen as the most favourable method for stimulating living cells. Artificially this can be easily done with silicon based circuits (transistors and capacitors) [13].

- Faradaic effect

External potentials near the plasma membrane of a living cell can induce faradaic currents through redox reactions. Faradaic currents can also contribute to the process of cell stimulation, however redox reactions are generating partially harmful molecules like H_2O_2 and should therefore be avoided [10].

- Thermocapacitive effect

The depolarisation with photothermal heating is caused by a temperature difference between the interior and exterior of the cell which therefore changes the membrane temperature. A change in plasma membrane temperature leads to a change in membrane capacitance and therefore to a change in membrane potential. This effect is called the "thermocapacitive effect" or the "photothermal effect" and is expected to be the leading effect in artificial light induced cell stimulation [4]. This effect is the main focus of this thesis and is described in detail in section 3.2.

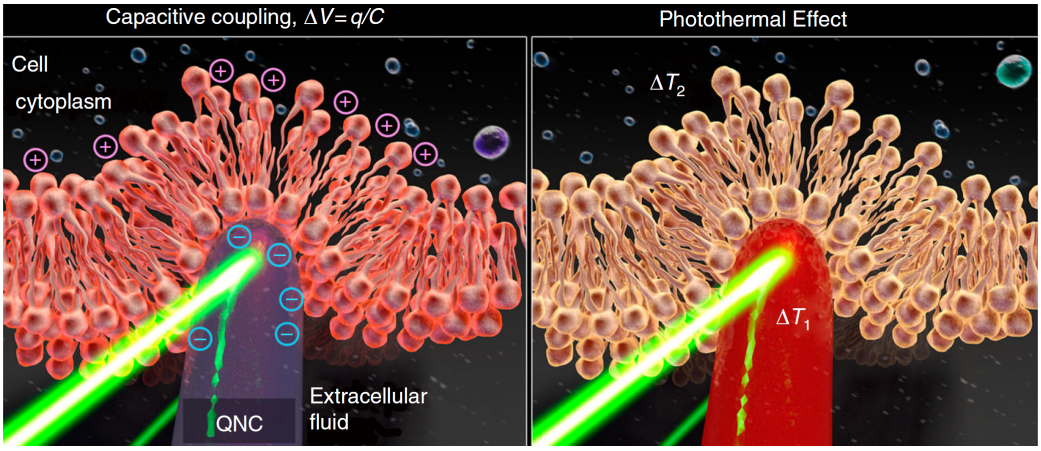

Figure 8: Illustration of the difference between the photothermal effect and the capacitive effect. The capacitive effect causes a charge carrier separation that induces a potential difference $\Delta V = q/C$. The photothermal effect is caused by a temperature difference between the interior and exterior of the cell which therefore changes the membrane temperature. [15, p.47]

3.2. Changing the membrane potential with temperature, the thermocapacitive effect

It has been shown that infra red light can be used in order to increase cell membrane temperature and therefore increase its electrical capacitance. [14] Similar to the model in section 3.1.1 we can draw an equivalent circuit, only this time we consider a time and temperature dependent capacitance $C_M(T(t))$ rather than a constant capacitance [3] (see fig. 9).

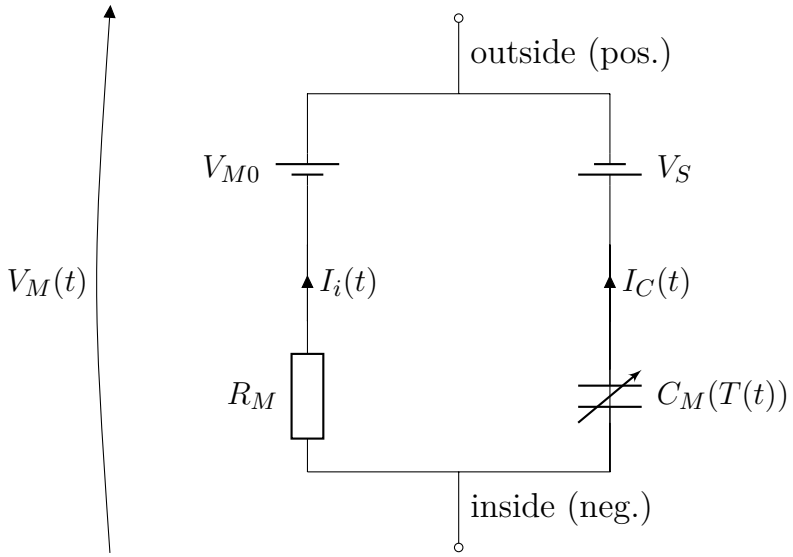

Figure 9: Electrical equivalent circuit of a living cell, with R_M the membrane resistance, $C_M(T(t))$ the temperature dependent cell membrane capacitance, $I_i(t)$ the current across the cell membrane resistance R_M, $I_C(t)$ the time dependent current across the capacitor, V_S the net surface potential of the membrane, $V_M(t)$ the time dependent total membrane potential across the whole cell and V_{M0} the reversal membrane potential which corresponds to the resting membrane potential in the resting cell membrane. [3]

Considering a time dependent capacitance and voltage across the capacitor V_C leads to a time dependent transmembrane charge difference,

$$Q_M(t) = C_M(t)V_C(t) = C_M(t)\big(V_M(t) - V_S\big). \tag{8}$$

Here V_S is the net surface potential of the membrane. With the time derivative and the chain rule the current across the capacitor $I_C(t)$ is then

$$\begin{aligned} I_C(t) = \frac{dQ_M(t)}{dt} &= V_C(t)\frac{dC_M(t)}{dt} + C_M(t)\frac{dV_C(t)}{dt} = \\ &= \big(V_M(t) - V_S\big)\frac{dC_M(t)}{dt} + C_M(t)\frac{dV_C(t)}{dt}. \end{aligned} \tag{9}$$

The ionic current $I_i(t)$ through the membrane depends on the resistance of the membrane R_M and the reversal membrane potential V_{M0}. This can be expressed as a Thevenin equivalent as

$$I_i = \frac{V_M - V_{M0}}{R_M}. \tag{10}$$

V_R is here the voltage drop across the resistor R_M. In the case of a resting cell, the sum of the ion currents is zero ($I_i + I_C = 0$), hence we can write equation (9) as

$$I_i + I_C = \frac{V_M - V_R}{R_M} + \big(V_M(t) - V_S\big)\frac{C_M(t)}{dt} + C_M(t)\frac{V_C(t)}{dt} = 0, \tag{11}$$

which can be used to express the dynamic of the total membrane potential $V_M(t)$:

$$\boxed{\frac{dV_M(t)}{dt} + \frac{\big(V_M(t) - V_S\big)}{C_M(t)}\frac{dC_M(t)}{dt} + \frac{\big(V_M(t) - V_R\big)}{C_M(t)R_M} = 0}\,. \tag{12}$$

This differential equation can be solved for $V_M(t)$ if the temperature and time dependent function $C_M(T(t))$ is known. An experimental model for the temperature dependence of the capacitance can be determined by the measurements of Taylor R. E. et al. in 1965 [16]. In this experiments the membrane capacitance changes by ≈ 1 % per degree K. Therefore a simple estimation for the capacitance change is

$$\frac{dC_m(T(t))}{dt} = \frac{d}{dt}\Big[C_0 + C_0\gamma\big(T(t) - T_0\big)\Big]. \tag{13}$$

Here $\gamma \approx 0.01$ and T_0 is a reference temperature. Combining equation (12) and (13) is thus

$$\frac{dV_M(t)}{dt} + \frac{\big(V_M(t) - V_S\big)C_0\gamma\dot{T}}{C_0 + C_0\gamma\big(T(t) - T_0\big)} + \frac{\big(V_M(t) - V_R\big)}{C_0 + C_0\gamma\big(T(t) - T_0\big)R_M} = 0. \tag{14}$$

This is the desired ordinary differential equation which can be solved for $V_M(t)$. [3]

3.3. Cell stimulation with laser light pulses

From the equation (12) one can see that a change in temperature leads to a change in capacitance which consequently changes the membrane voltage (also called "optocapacitance"). The term $^{dC_M(T(t))}/_{dt}$ implies that not only the absolute temperature change but also a rapid change in capacitance therefore leads to membrane depolarization (see fig. 10). This effect can be used to depolarize living cells by heating up structures connected to the cells with light pulses. In equation (13) the value $(T(t) - T_0)$ is proportional to the power P of an incident (laser) light beam:

$$\big(T(t) - T_0\big) = PF(t) = \frac{E}{\Delta t} F(t). \tag{15}$$

The function $F(t)$ describes the time dependence of the temperature change $(T(t) - T_0)$ generated by a (laser) light pulse of the power P at the surface of a structure. The power P can be expressed over the total energy E of the laser pulse and the pulse duration Δt. With this the capacitance $C_M(t)$, from equation 13, can be written as

$$C_m(T(t)) = C_0 + C_0 \gamma E \frac{F(t)}{\Delta t}. \tag{16}$$

$F(t)$ also contains the geometry of the structure and the specific material properties. The function $F(t)$ is the solution of the heat equation

$$\frac{\partial^2 F(T(t, \mathbf{x}))}{\partial \mathbf{x}^2} + \frac{A_0}{k} = \frac{1}{\alpha} \frac{\partial F(T(t, \mathbf{x}))}{\partial t}, \tag{17}$$

where A_0 is the heat generated by a pulse of light, α is the thermal diffusivity of water, k is the thermal conductivity of water and $\mathbf{x}$ is a three dimensional location vector. In general this partial differential equation is hard to solve especially for complex geometries and materials.

Carvalho-de-Souza et al. [3] did the calculation for gold nano particles (AuNPs). They solved the equation (17) for AuNPs with the radius b:

$$(T(b,t) - T_0) = cP\left\{\sqrt{\frac{t}{\alpha\pi}}\left(b\ \exp\left[\frac{-b^2}{4\alpha t}\right]\right) + t - \left(t + \frac{b^2}{2\alpha}\right)\operatorname{erfc}\left[\frac{b}{2\sqrt{\alpha t}}\right]\right\} = \frac{E}{\Delta t}F(t). \tag{18}$$

Here the constant c includes the material specific properties [4].

In order to stimulate a living cell with a (laser) light pulse, it is important to estimate the pulse energy and pulse duration needed to trigger an action potential. For very high membrane resistance R_M equation (14) can be solved analytically for $V_M(t)$. Then the energy needed to exceed the threshold voltage V_{Th} (assumed constant) is

$$E_{Th} = \Delta t\ \frac{V_R - V_{Th}}{\gamma F(t)(V_{Th} - V_S)}. \tag{19}$$

For small values of t (in the range of 1 s to 10 ms) and with the approximation $b^2 \gg \alpha$ the equation (18) gives us the interesting relation:

$$\boxed{\big(T(t) - T_0\big) = PF(t) = cP\sqrt{t}}\ . \tag{20}$$

[4] c can include absorption properties e.g. the fractional occupancy and the plasmon resonance properties of AuNPs.

By replacing $F(t)$ in equation (19) we get

$$\boxed{E_{Th} = \frac{\Delta t}{\sqrt{t}} \frac{V_R - V_{Th}}{c\gamma(V_{Th} - V_S)}} \,. \tag{21}$$

We see that there is less total energy E_{Th} required to reach the threshold energy with shorter pulse duration. The energy needed to trigger action potentials with temperature is therefore [3]:

$$\boxed{E_{Th} \propto \sqrt{\Delta t}} \,. \tag{22}$$

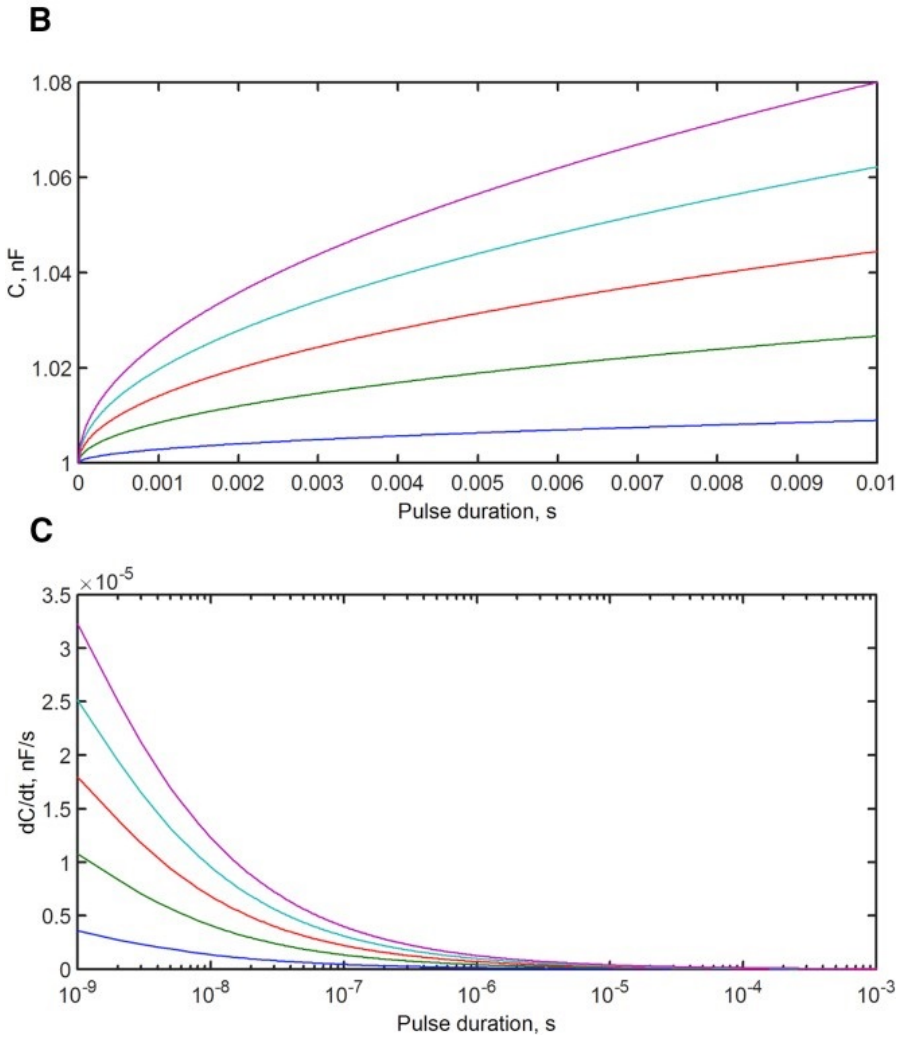

Figure 10: Simulation of the time dependence of the optocapacitive effect. (B) Plot of equation (16) including the modelling of the function $F(t)$ for gold nano particles heated up with 532 nm laser light pulses of duration Δt and different powers P. (C) Plot of the time derivative of C_M predicting the ionic current I_C across the capacitor. [3]

4. Organic semiconductor structures

Organic semiconductors in general are π-bonded molecules or polymers consisting of carbon, hydrogen and occasionally elements like nitrogen, oxygen, sulfur, chlorine and bromine. The band gap of an organic semiconductor is typically $2.5 - 4\ eV$ while the band gap in conventional semiconductors, like in silicon, is typically $1 - 2\ eV$. The band gap of the organic semiconductor is here the energy region between the HOMO (highest occupied molecular orbital) and LUMO (lowest unoccupied molecular orbital) of the organic semiconductor molecules. At room temperature the electrical properties of organic semiconductors show more similarities to insulators than to semiconductors. The electrical behaviour however changes, when charge carriers are either injected or generated by doping or optical excitation [17].

4.1. 3-D structured semiconductor pigments for artificial cell stimulation

One of the key properties of organic semiconductors used for artificial cell stimulation are the bio-compatible interface between the semiconductor structure and the cell membrane [15]. Therefore it is important to use organic semiconductor molecules which are capable of forming a suitable 3-D micro-structure. For this purpose the well known organic semiconductors tetracene ($C_{18}H_{12}$) and pentacene ($C_{22}H_{14}$) have been reported as suitable.

Tetracene, a four ringed acene and pentacene, a five ringed acene, are aromatic hydrocarbons. Their H-bonded analogs epindolidione and quinacridone, with additional amine (NH) and carbonyl (CO) groups, tend to form a solid state crystal structure, as they form an inter-molecular bonding between adjacent molecules (see figure 11). The nanocrystalline form of epindolidione and quinacridone are commonly used as dyes in inkjet printings. Epindolidione is a

yellow colorant and quinacridone is a common magenta dye. Furthermore, as they are used in cosmetics and paints their non-toxicity is validated and they are proven bio-compatible [7].

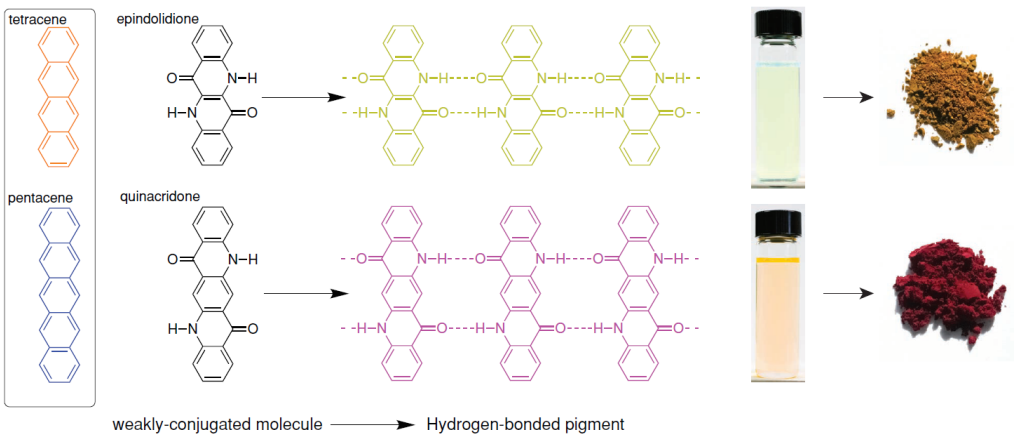

Figure 11: The organic semiconductors tetracene and pentacene are the four and five ringed aromatic hydrocarbons that belongs to the series of acenes. Their analogs with carbonyl and amine groups tend to form H-bonded solid state crystals which are commonly used as dyes in paints, cosmetics and inkjet printers [7].

4.2. Optical end electrical properties of epindolidione and quinacridone

The solid state forms of epindolidione and quinacridone show different physical properties to their isolated molecule form. Especially the optical properties change with the crystallisation process. Quinacridone is pale yellow in dilute solution and red to purple as crystallite [7].

The absorption coefficient α is important in respect of generating heat for cell membrane stimulation (see figure 12). Solid state quinacridone thin films roughly absorb light in the range of 500 to 600 nm wavelength with a strong peak at ≈ 570 nm and smaller peak at ≈ 535 nm. For Quinacridone structures

this seems to depend on the crystalline phase structure i.e. the different crystal phases α_2, β and γ have been reported to show slightly different absorption coefficients [15]. Solid state epindolidione thin films absorb in the range of 400 to 520 nm wavelength with a strong peak at ≈ 490 nm and smaller peak at ≈ 455 nm [7].

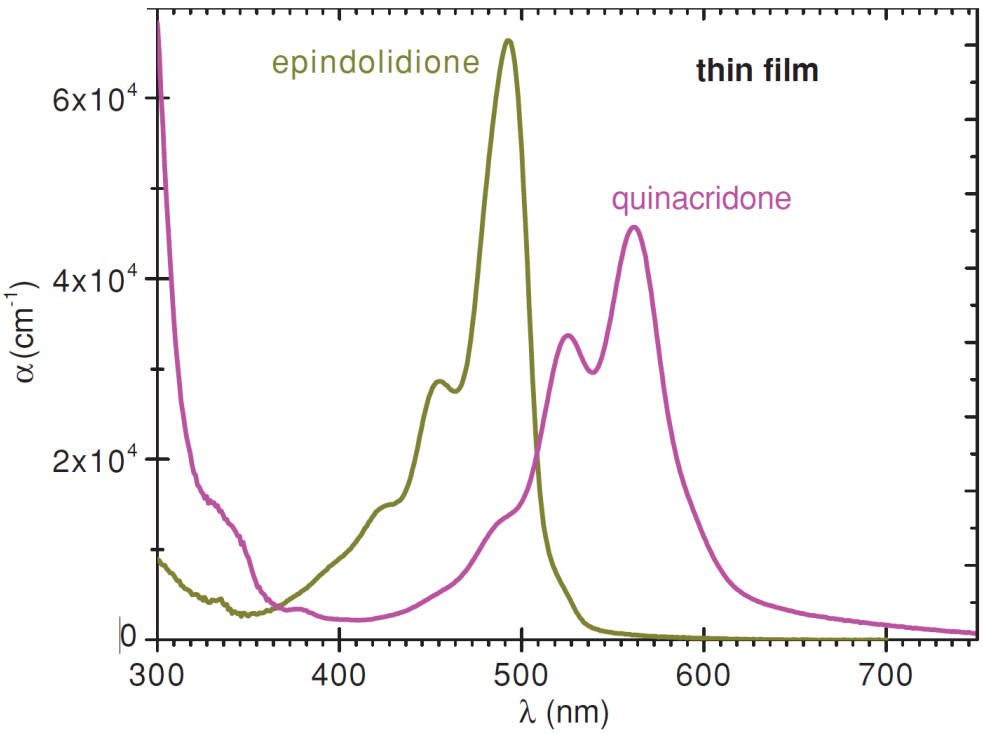

Figure 12: Absorption coefficient α of epindolidione and quinacridone crystalline thin film [7].

Quinacridone and epindolidione can be used in organic field effect transistors (OFETs) with (air-) stable operation times of over 140 days. Quinacridone and epindolidione show hole mobilities of $\mu_Q = 0.2$ cm^2/Vs and $\mu_E = 1.5$ cm^2/Vs. Quinacridone seems to be slightly more stable than epindolidione, however epindolidione shows a 7.5 times higher hole mobility and hence increased conductance (see figure 13 and 14) [7].

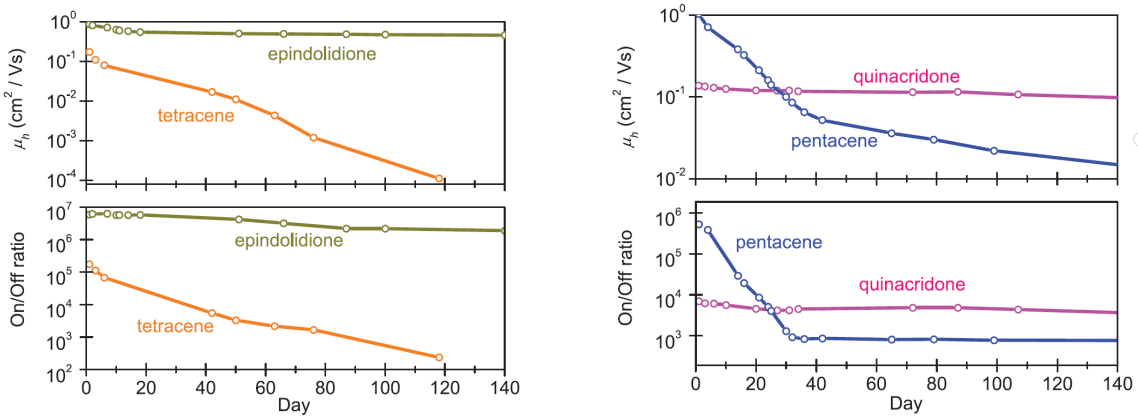

(a) (b)

Figure 13: Electrical performance, On/Off ratio and hole mobility μ_h, of organic field effect transistors (OFETs) made out of (a) epindolidione/tetracene and (b) quinacridone/pentacene [7]

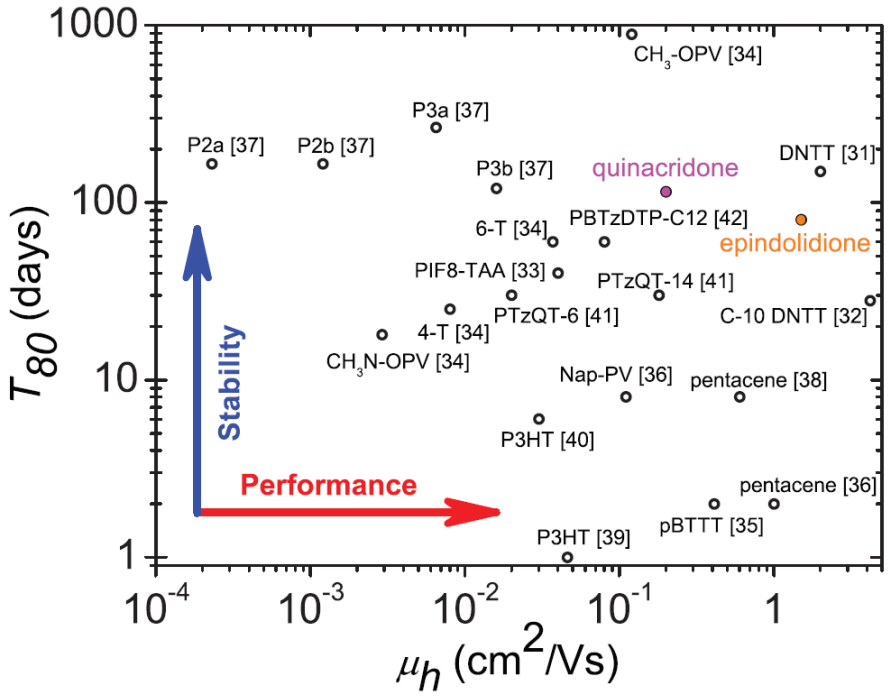

Figure 14: Comparison of the hole mobility μ_h and the stability of quinacridone, epindolidione, tetracene and pentacene. The time T_{80} is the lifetime of an OFET where the charge mobility is 80% of the initial value [7].

4.3. Photothermal heating of qinacridone micro structures with laser light pulses

As we know from the differential equation 12 in section 3.2 the change of the cell membrane potential $C_m(T(t))$ depends on the change of the capacity of the cell membrane. Since the capacity is temperature dependent, as you can see in equation 13, a fast change in membrane temperature is important to efficiently trigger action potentials in cells. This can be achieved on the one hand with short and intense light pulses (see figure 15), as shown in equation 21, and on the other hand with fast heat dissipation within the connected structure.

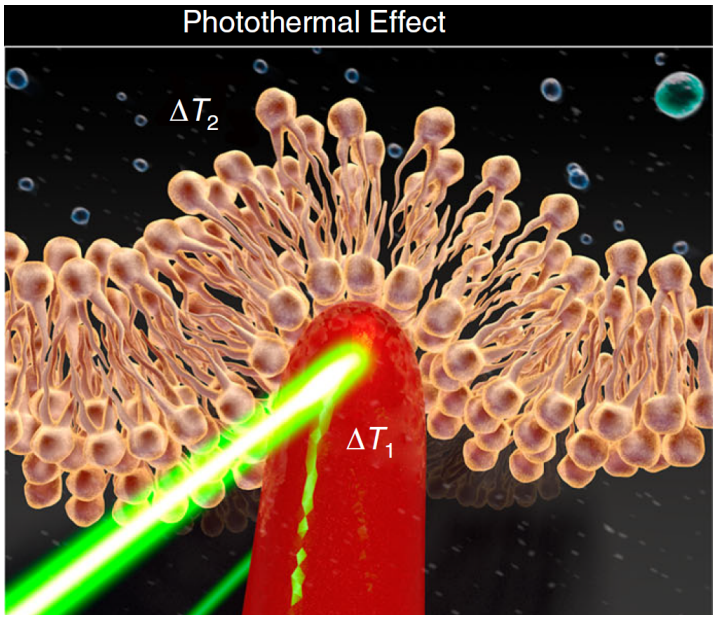

Figure 15: Illustration of the photothermal effect caused by a laser light pulse focused on a quinacridone micro structure in contact with a cell membrane. The absorption of the laser light ΔT_1 leads to a temperature difference between the quinacridone structure T_2 and the interior of the cell T_1 and heating T_2 of the interior of the cell. [15]

Finite element method simulation (FEM-simulation) [5] has shown that a quinacridone hedgehog structure with a radius of $r \approx 4\ \mu m$ can heat up by $\Delta T \approx 4\ ^{\circ}C$ in less than $\Delta t = 0.1\ s$ by applying a 20 $^{mW}/_{cm^2}$ laser pulse over the duration of $\Delta t = 1\ s$. The boundary conditions included a heat dissipation that was assumed to be a convective heat flux within the water environment with a heat transfer coefficient of 40 $^{W}/_{m^2K}$.

As it can be seen in figure 16 the heat dissipation in a quinacridone hedgehog structure happens four times faster than in a spherical quinacridone structure of the same size and almost as fast as in a 50 μM by 50 μM planar quinacridone layer with 0.32 μm thickness.

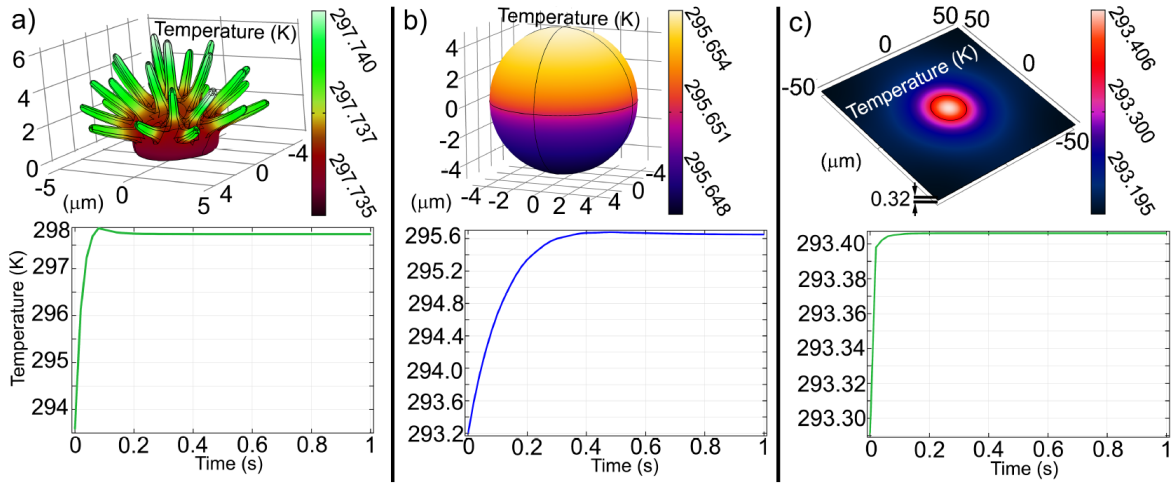

Figure 16: Finite elements method simulation of the heat equation for different quinacridone micro structures. The heat was induced with a 20 $^{mW}/_{cm^2}$ laser pulse over the duration of $\Delta t = 1\ s$. The heat dissipation was assumed to be convective heat flux with a heat transfer coefficient of 40 $^{W}/_{m^2K}$. The simulation has been done with the COMSOl Multiphysics 4.2a software (COMSOL Inc.). a) Heat dissipation for a quinacridone hedgehog structure with a radius of $r \approx 4\ \mu m$. b) Heat dissipation for quinacridone sphere with a radius of $r \approx 4\ \mu m$ c) Heat dissipation for a 50 μ by 50 μ planar quinacridone layer with 0.32 μm thickness. [15]

[5] Finite element method (FEM) is a numerical method for solving partial differential equations (PDEs) by approximating the PDE locally with a set of ordinary differential equations (ODEs) on a grid covering a geometric object.

4.4. Quinacridone hedgehog structures forming an interface with HEK cells

In 2017 M. Sytnyk et. al. showed that quinacridone hedgehog structers form close interfaces with HEK (Human Embryonic Kidney cancer cells [6]). On the one hand a close interface and a large contact area with the cell membrane is important as this maximizes the effects of cell stimulation, on the other hand it is important that the structures are small enough to be heated efficiently by laser light pulses i.e. the light pulses should heat up the structure fast enough. Electron microscopy images have shown that the size of the hedgehog structures can be varied from $2\mu m$ to $20\mu m$, depending on the synthesis method.

The interface between HEK cells and quinacridone nanohedgehog structures increases over cell culture time (see figure 17 top images) as the cells tend to overgrow the structures. This is very likely attributed to the geometry of the structures and their ability to form very close interfaces with the cell membrane. As shown in figure 17 (bottom image) the "nanodaggers" of the structure in some cases form gaps of few nanometers and even penetrate parts of the cell membrane. [15]

[6] Human embryonic kidney 293 cells, also called HEK cells, are a cell line originally from human embryonic kidney cancer cells. They can be grown (multiplied) in cell tissue culture.

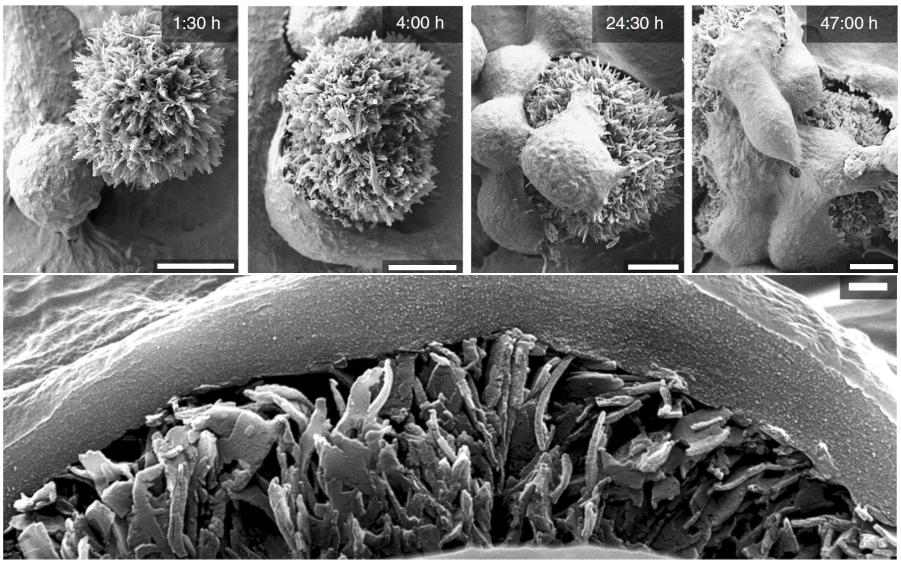

Figure 17: The top electron microscopy images show the growth of HEK cells over the duration of $1:30\ h$ to $47:00\ h$ (scale bar top images $= 2.5\ \mu m$). The bottom image shows a magnification of the quinacridone structure and cell membrane interface. The nanodaggers of the quinacridone structure form gaps of a few nanometers and even penetrate parts of the cell membrane. (scale bar bottom image $= 500\ nm$) [15]

4.5. Epindolidione hedgehog structures forming an interface with neurons

Analogue to quinacridone structures epindolidione organic nano-architecture pigments have been synthesised from H-bonded tetracene (in cooperation with Prof. Dr. Wolfgang Heiss et. al., Friedrich-Alexander University Erlangen-Nürnberg). Similar to quinacridone it is possible to manufacture different designs and crystal phases with epindolidione. Depending on the crystal phase this particles show more favourable optical (absorption wavelength, absorption coefficient and quantum yield) and electrical (hole and electron mobility μ_h) material properties.

To show that epindolidione nano-architectures are capable of forming tight and "voluntarily" interfaces with living cells, the pigments have been seeded with

embryonic rat cortex neurons and then kept in cell tissue culture. Electron microscopy imaging gives evidence for the size and architecture of the organic semiconductor structures as well as a feeling for the neuronal growth (kindly provided by Prof. Gerd Leitinger and Karin Kornmüller, PhD, Med. University of Graz). As it can be seen in figure 18 and 19 the particle size is roughly between 2 μm and 10 μm. This images have been taken with a scanning transmission electron microscope (STEM) with a secondary electron detector (SE-detector).

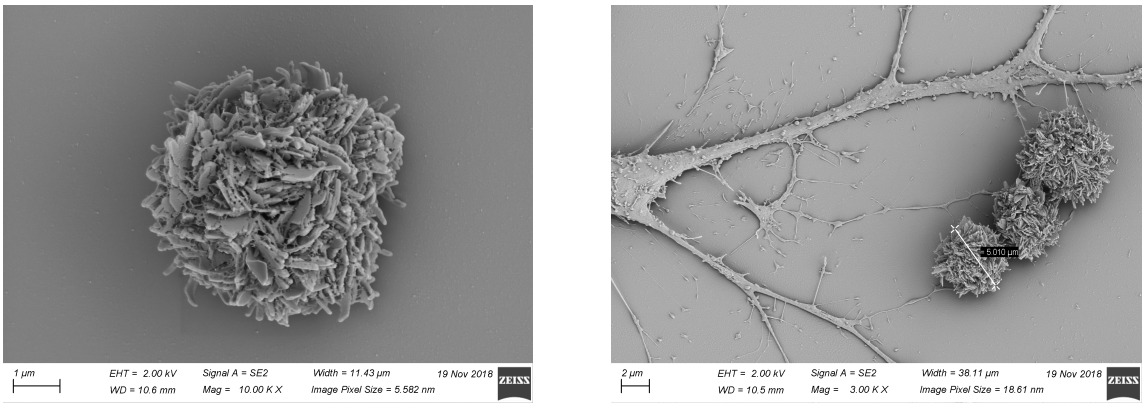

(a) (b)

Figure 18: Electron Microscopy images of the H-bonded epindolidione molecules forming a nano-architecture pigment. (a) A single particle epindolidione particle at a magnification of $Mag = 10.00\ K\ X$ shows the surface structure of the pigment. (b) Measured size of one of the particles is at roughly 5 μm. The particles seem to be in contact with the dendritic branches of a neuron

The neurons clearly show a tendency to grow their dendritic branches [7] in the direction of the organic semiconductor pigments (see figure 19 (a) and (b)).

[7]Neurons essentially consist of three parts:
1) The soma, the body of the cell.
2) The dendrites: Cellular expansions of the neuron which tend to form interfaces with other neurons. The dendrites (and the smaller tips the dendritic branches) are responsible for the electrical input.
3) The Axon: A single longer and thicker version of the dendrite that is responsible for the electrical output of a neuron.

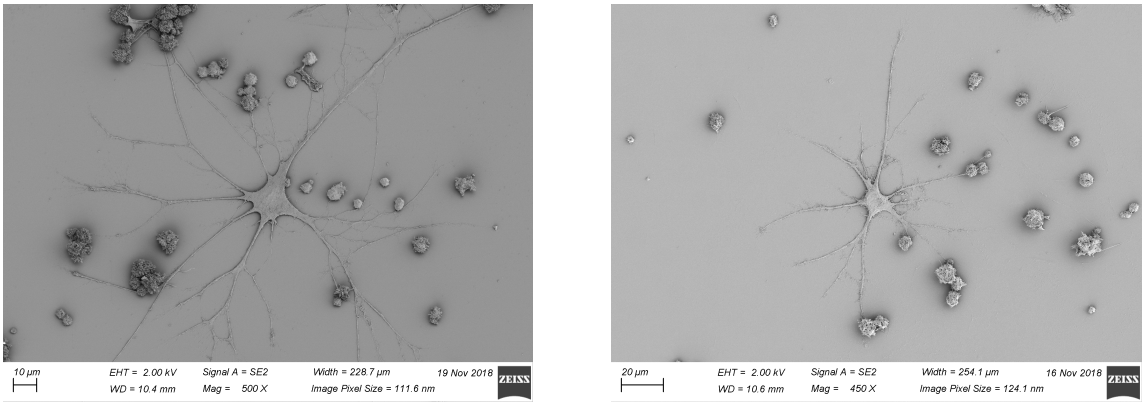

(a) (b)

Figure 19: Electron microscopy image of embryonic rat cortex neurons seeded with epindolidione hedgehog structures. The images show the dendritic branches of the neurons that partly advance to the pigments.

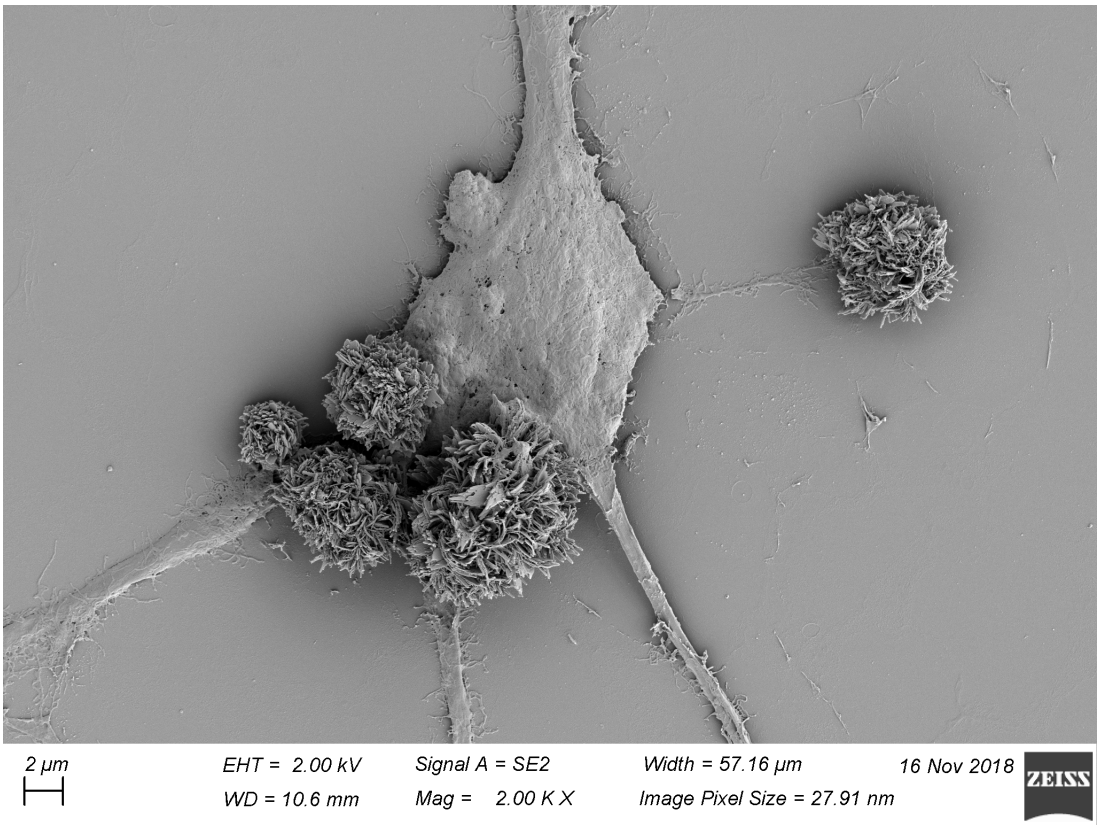

Figure 20: Different sizes of epindolidione hedgehog structures in contact with the soma of an embryonic rat cortex neuron.

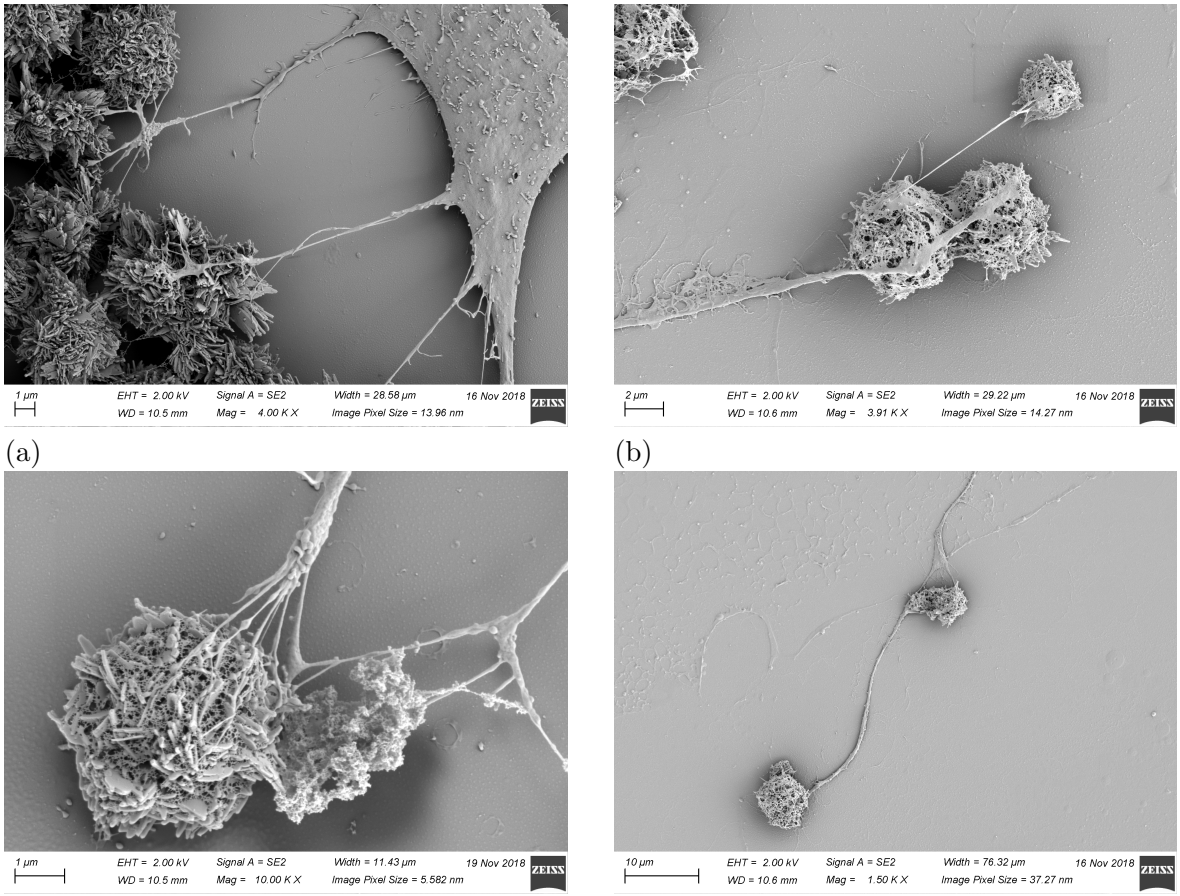

Figure 21: Dendritic branches of embryonic rat cortex neurons advance to the epindolidione hedgehog pigments and form a strong interface.

A lot of effort is needed to produce a suitable biological sample for electron microscopy. To be able to conserve the biological structure of the neurons the cells have to be stained (e.g. with osmium tetroxide OsO_4) and dehydrated (with liquid ethanol and aceton followed by critical point drying). SEM imaging and suitable sample preparation allows to provide high resolution images of the neuronal interface with the organic semiconductors.

5. Experimental setup

5.1. Sketch of the setup and devices

The experimental setup for electrophysiological recordings in living cells by laser induced stimulation is depicted in figure 22 with the devices from 1.

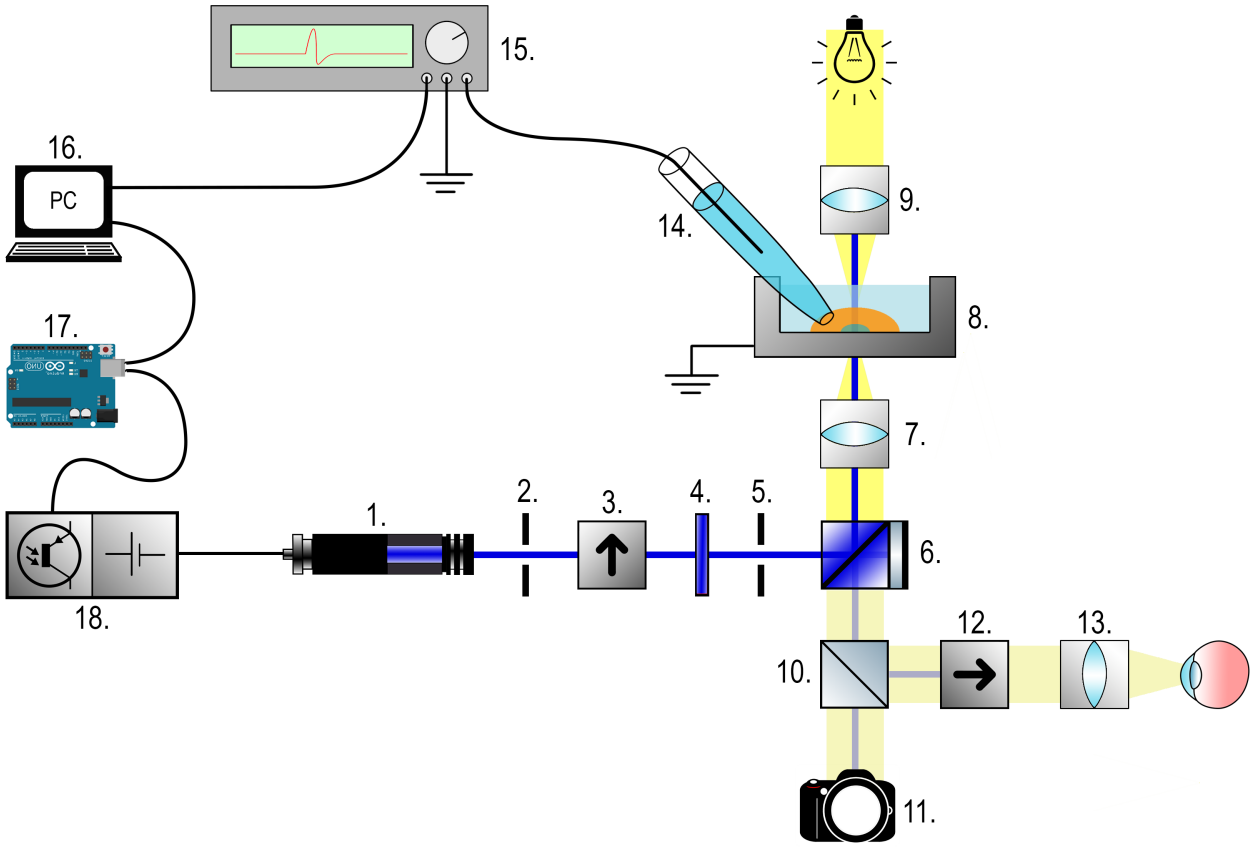

Figure 22: The experimental setup for electrophysiological recordings in living cells by laser induced stimulation. 1. solid state laser 450 nm, 2. aperture and laser collimator with adjustable distance to the laser outlet, 3. dichroic film polarizer, 4. Band-pass filter 450 nm, 5. adjustable iris diaphragm aperture, 6. dichroic mirror, 7. objective lense, 8. sample holder, 9. light source with collimator and apertures, 10. beam splitter, 11. camera mounted to microscope, 12. dichroic film polarizer, 13. eye piece with magnifying lense, 14. patch pipette with electrode and head stage pre amplifier, 15. patch clamp amplifier and digitizer, 16. PC with C++ script for laser control and for recording data, 17. programmable micro controller, 18. circuit for controlling the laser.

5.2. Device list

Table 1: Devices for the setup with numbers from figure 22.

#	**Device**	**Characteristics**
1	Laser	10 W solid state laser pointer, wavelength $\lambda = 450\ nm$, max operating voltage DC $V_L = 7.4\ mV$
2	Aperture and collimator	Aperture and collimator for the laser pointer with adjustable distance to the laser outlet
3	Polarizer	Dichroic film polarizer sheet, $400 - 700\ nm$, 360° adjustable
4	Band-pass filter	Center wavelength $CWL = (450 \pm 8)\ nm$, full width half max $FWHM = (40 \pm 8)\ nm$, blocking $200\ nm - 1150\ nm$,
5	Aperture	Adjustable iris diaphragm aperture
6	Dichroic mirror	Dichroic mirror with reflection and transmission in the range of the laser light ($450\ nm$)
7	Objective lenses	objective lenses: 1. Nikon Plan Flour 40x WD 0.72 DICM ∞/0.17, 2. Nikon Plan Flour 20x WD 2.1 DICN2 ∞/0.7, Nikon Plan 4x
8	Sample holder	Grounded sample holder with a bath for living cells and physiological solutions
9	Microscope collimator	Collimator, apertures and light source for microscopic imaging
10	Beamsplitter	Beamsplitter for splitting the optical beam path to the camera and the eye piece
11	Camera	Spot Imaging scientific camera with cooled (TEC) CCD chip INV: 3000015730000
12	Polarizer	Dichroic film polarizer sheet, $400 - 700\ nm$, 360°, built in the eye piece, adjustable for gradually blocking the laser
13	Eye piece	Eye piece with either the polarizer 12 or a x10 magnifying lense
14	Patch pipette	Glass patch pipette with head stage preamp 'Axon CNS CV 203BU' and silver-silver chloride ($Ag/AgCl$) reference electrode
15	Amplifier and digitizer	Patch clamp amplifier 'Axon CNS Axopatch 200B' and AD converter 'Axon CNS Digidata 1440A'
17	Micro controller	'Arduino Genuino MEGA2560 SainSmart MEGA 2560 R3 AVR' micro controller
18	Laser control circuit	Custom built circuit for switching the laser on and off with an Arduino protocol
-	Microscope	Nikon Eclipse TE300

5.3. The setup assembly

The experimental setup is shown schematically in figure 22 with the devices from table 1. Generally the setup consists of four main parts:

1) The laser unit

The laser assembly with the laser pointer, apertures, a filter and a polarizer.

2) The microscope

The microscope with a camera, a polarizer and a dichroic mirror.

3) The setup for electrophysiological recordings

The glass pipette on a micro manipulator with an electrode, a sample holder, a pre amp head stage, a patch clamp amplifier and a patch clamp digitizer.

4) The laser controlling circuit

A circuit to regulate on/off voltage and power for the laser. This also includes a computer and a programmable micro controller.

The first part is build from a dismantled laser pointer. This solid state laser has 10000 mW output intensity and a direct current operating voltage of $V_L = 7.4\,mV$. The laser light has an intensity peak at wavelength $\lambda = 450\,nm$ (blue). The laser is mounted in a device that was originally a collimator for an external light source for the microscope. Therefore, it can easily be mounted on the back of the microscope. This builds a stable portable unit (see figure 23) so that additional optical elements can be placed in the optical path. Behind the laser source there is a laser collimator lense with an aperture. This lense is variable in length to force the divergent laser light into a parallel light beam with a focal length of infinity ($f = \infty$). Directly behind the collimator is a 360° adjustable dichroic thin film polarizer sheet. This polarizer ensures linear polarization of the laser light beam with a variable plane. The next element in the beam path

is a narrow band-pass filter with a center wave length of $CWL = (450 \pm 8)\ nm$ and a full width half max of $FWHM = (40 \pm 8)\ nm$. This filter blocks every possible harmful wavelength as the laser pointer is suspected to emit laser light in the infra red as well as in the ultraviolet range. The last element in the beam path of the laser unit is an iris diaphragm aperture with adjustable pin hole size and two screws to adjust the pin hole in a $x-y-plane$ normal to the beam path.

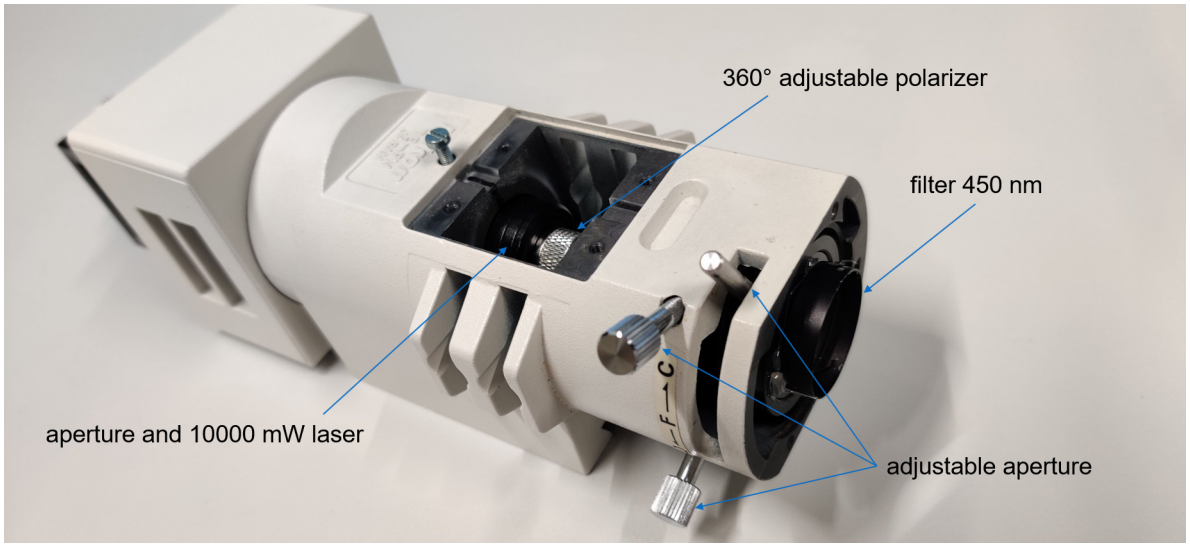

Figure 23: The laser unit with an 10000 mW solid state laser with wavelength $\lambda = 450\ nm$, an aperture with collimator, an 360° adjustable polarizer thin film sheet, a narrow band-pass filter at $\lambda = 450\ nm$ and an adjustable iris diaphragm aperture.

The second part of the setup consist of an inverted Nikon Eclipse TE300 microscope with an additional inlet from the back. From this inlet the laser beam enters the microscope and gets deflected upwards from a 45° dichroic mirror (see figure 22). The dichroic mirror has been chosen to not fully deflect the laser light beam upwards into the objective so that a small percentage of the laser light beam is guided downwards to a beam splitter to make the laser light spot visible on the camera. With a C-mount the camera is directly mounted to the side of the microscope. The camera is hooked to the PC to give a live image

while working with a sample. With the camera it is possible to align the beam in the 2D-plane of the sample in order to directly focus onto a preferred structure. Unfortunately the beam splitter also guides some of the remaining laser light into the eyepiece. To minimise health hazards there is a second adjustable polarizer thin film sheet placed in the eye piece which is 90° to the first polarizer to cancel out any remaining laser light.

Please Note: Even though the laser light is weakened significantly and is filtered properly, eye protection with an absorption wavelength of 450 nm must be worn while operating the laser at any time. The laser is a class IV laser which means the direct and indirect laser light is hazardous to view under any condition without protection [1].

The majority of the laser light beam is guided upwards from the dichroic mirror into the objective lense. As the laser light is a parallel beam the objective lense automatically focuses the laser spot onto the 2D-plane of the sample holder, thus the laser point is in the same focus as the sample, regardless of the objective being used. The objectives are located on an objective revolver. For this experimental setup three different objectives can be used with either 40x, 20x and 4x magnification. For a maximum intensity per area laser spot it is therefore advised to use the 40x magnification objective.

The third part of the setup is the equipment for electrophysiological recordings (see section 3.1.2). The patch clamp setup consists of an electrical circuit with a glass pipette, an electrode, a head stage pre amplifier, a patch clamp amplifier, a digitizer and an electrode in the electrolyte bath of the sample holder. The patch clamp pipette is a pulled glass pipette with a tip resistance of $R_p \approx M\Omega$. Inside the pipette is a silver silver-chloride electrode ($Ag/AgCl$) which is in contact with an electrolyte inside the pipette. As this setup should be capable of measuring currents in the range of a few picoampere and potentials in the

range of millivolts it is important to mount a head stage pre amp directly to the electrode to reduce noise and losses due to long cables. The head stage amp is directly grounded via the bath reference electrode to minimize the circuit size. The increased signal from the head stage is then further fortified via the patch clamp amplifier. The patch clamp amplifier is also used to switch between voltage clamp mode and current clamp mode and to adjust the zero potential. The analog signal coming from the patch clamp amplifier is then converted to a digital signal using a digitizer with 250 kHz per channel.

The fourth part of the setup, the laser controlling circuit, consists of a programmable micro controller (Arduino), a circuit for fast switching and a power source for the laser 24. The main part of the custom built controlling circuit is a high capacity PhotoMOS-Relay (Photo Metal Oxide Semiconductor Relay). Using the PhotoMOS-Relay it is possible to switch the power supply for the laser with a digital signal coming from the Arduino. A PhotoMOS-Relay has fast switching times compared to a conventional relay, which makes relatively short laser pulses feasible. To control the laser pulses it is possible to load a C++ script onto the Arduino. This adds the option to customize the protocol that runs the laser in order to sync it to the patch clamp setup (e.g. with TTL logic). It is also possible to change the output intensity of the laser by applying less voltage. Therefore the power supply has a variable output voltage.

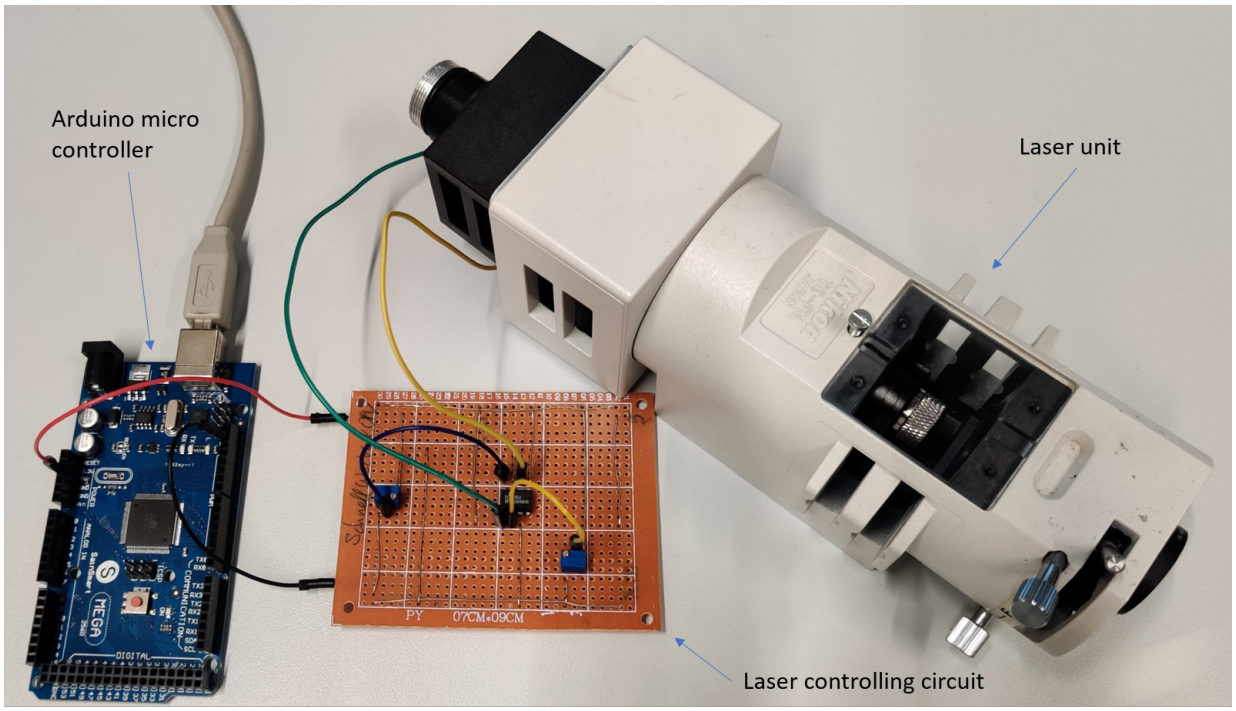

Figure 24: Arduino with programmable C++ script sends a digital signal to the laser controlling circuit (here without the power supply). The laser controlling circuit with a high capacity PhotoMOS-Relay is used for fast on and off switching of the laser light power.

6. Experiments and results

6.1. Quantitative analysis of embryonic neuron growth on epindolidione structures

To visualize the dynamics of neuronal interface with the epindolidione structures in live cell experiments, we monitored the neuronal migration and interaction using a life cell observer. The live cell observer provides a physiological environment for the neurons with body temperature and controlled CO2 levels to balance the pH of the cell media. Sequential images of neurons are processed at various predefined spots of the well plate over the time course of 72 hours.

The important question is, if the neurons tend to form an interface with the epindolidione hedgehog structures over the duration of the videos. To proof this behaviour statistically, single dendrites have been traced with a Fiji(ImagJ distribution) plugin "Simple Neurite Tracer" [12]. This analysis results in a set of matrices, which contains the spatio-temporal coordinates (x, y and t values) of the dendritic growth.

For further evaluation of the data a Matlab script has been written to statistically analyse the dendritic growth (see appendix A). Figure 25 (A) shows the process of tracing the embryonic neuron growth and the translation of this information into a Matlab script (B). In the example figure 25 (C) the dendritic endpoint growth over time shows a cluster of endpoints over time at specific coordinates where epindolidione particles are located. By integrating over the path of the dendrite one can estimate the total length l_{tot} of the dendrite over time (see figure 27). In this example we see that the dendrite grows fast in the first 10 hours and eventually stops growing when it comes in contact with the hedgehog structures. By subtracting the total length at time step t_n from the time step t_{n+1} we can define a dynamic d for the dendrite (see figure 27):

$$d = || \, l_{tot}(t_n) - l_{tot}(t_{n+1}) \, || \tag{23}$$

Areas with low dendritic dynamic could be used to show that dendrites exhibit less growth and movement while docking events with organic semiconductor structures occur.

Please Note: The evaluation in this section (section 6.1) has been done with the growth of one example dendrite in one video. To make a statistical significant statement regarding the behaviour of embryonic neurons, a much greater sample of neuron tracings and quantitative and statistical analyses have to be conducted.

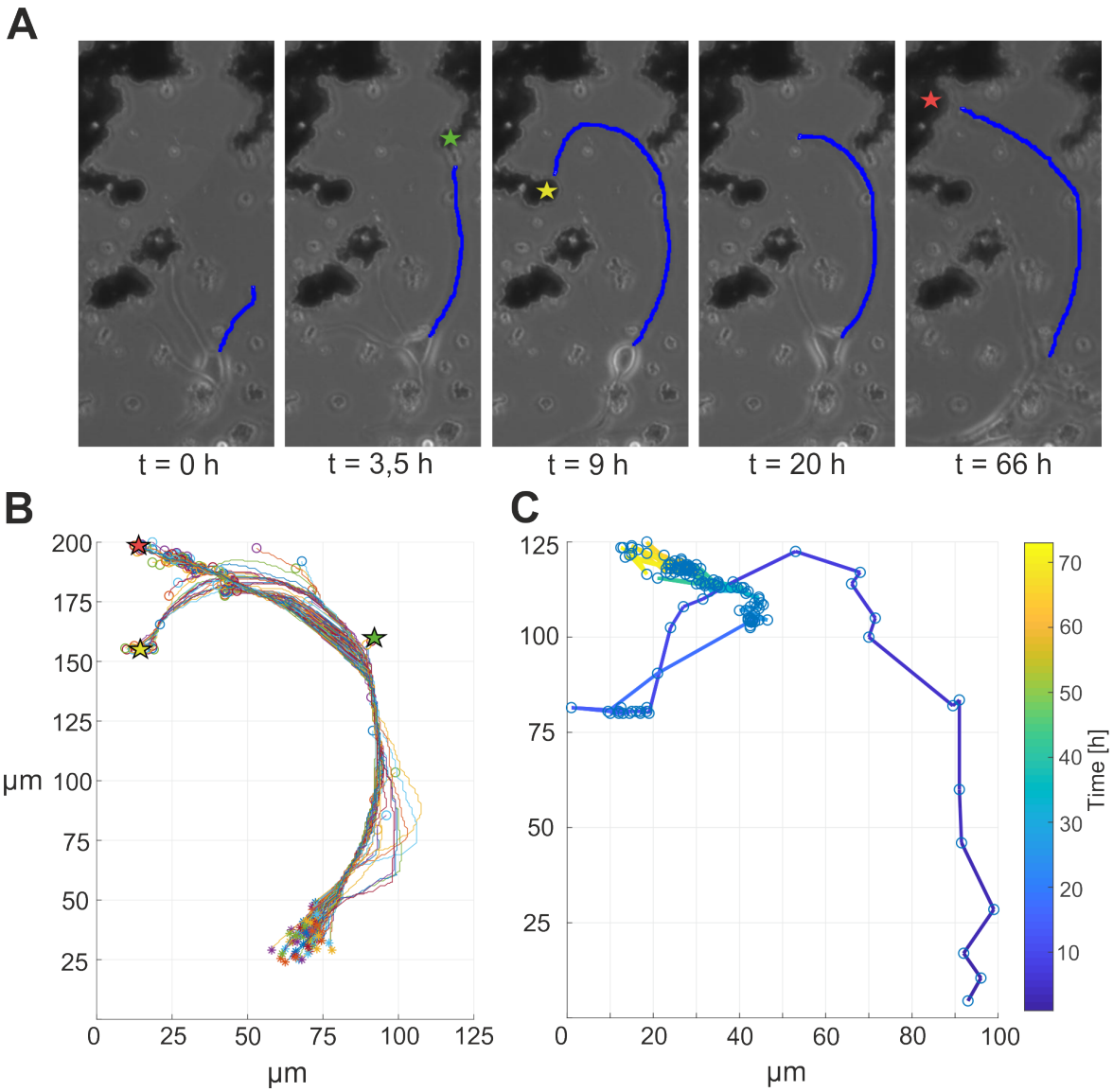

Figure 25: (A) Example pictures of a video recorded with the live cell observer overlayed with the corresponding traces. The star indicates a possible docking event of the dendritic endpoint with hedgehog structures. (B) The total dendritic traces for every time step over the course of 72 h. The o-marker depicts the endpoint of the dendrite. (C) Location of the dendritic endpoint over time (time steps of $\approx$ 20 min).

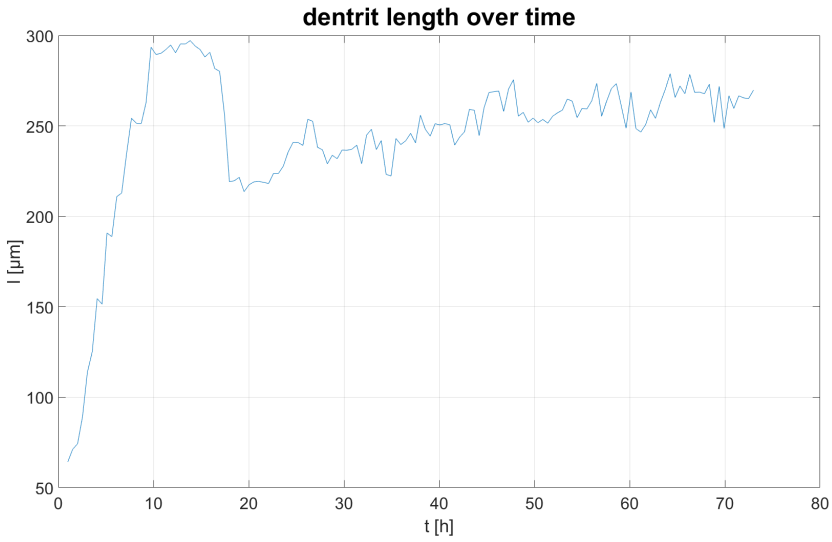

Figure 26: The total length l_{tot} over time of the example dendrite shown in figure 25 (A)

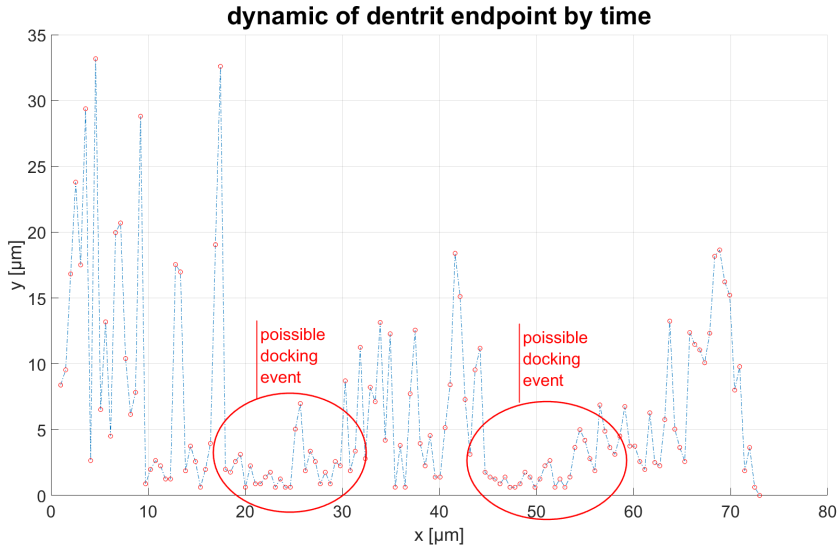

Figure 27: The dynamic d over time of the example dendrite shown in figure 25 (A). In this example the 2 areas of low dynamic could indicate a docking event between dendrite and semiconductor structure.

6.2. Operating the laser in the experimental setup

In order to efficiently stimulate the plasma cell membrane it is important to focus the laser directly onto the 2-D plane of the sample. As the laser is set up to be a parallel beam the laser point should be automatically focused via the objective lense. Therefore the dimension of the beam in the sample plane depends on the objective lense used and can be varied depending on the application. With very low laser operation intensity (operating voltage under $\approx 3\ V$ DC) it is possible to move the image of the laser point onto a desired location in the sample. Here the laser needs to be in a permanent ON-mode, since the laser pulse time is shorter ($\Delta t \approx 10 - 100\ ms$) than the reaction time of the camera ($\approx 10 - 20$ frames per second, depending on the operation options). The laser point needs to be adjusted with the camera as it is not possible to see the laser point through the eye piece of the microscopy because of the polarisation filters and the safety goggles (see section 5.3 safety hazards).

Alternatively it is possible to arrange the laser spot in the sample plane by using a fluorescent sample. Here we saw that the epindolidione structures are clearly fluorescent under blue ($\lambda = 450\ nm$) light. This is also good estimation if (and with how much intensity) the laser spot is hitting the organic semiconductor.

Figure 28 shows an image of the laser spot focused on a sample holder with living cells. The spheres in the background are HEK-cells with a typical diameter of approximately 10 μm. In this configuration (low laser intensity, objective lense with magnification of x40 and adjustable iris diaphragm aperture 5 see table 1) the spot is roughly half of a HEK-cell, $\approx 5\ \mu m$ length and $\approx 1\ \mu m$ width. With a smaller aperture setting and a higher magnification the spot size can be chosen smaller, however a smaller aperture setting results in a lower laser intensity. For the option of a smaller laser spot the output laser power has been chosen significantly higher than the experiment requires. Additionally the laser

spot size is limited by diffraction as the aperture diameter must be higher than the wavelength of the laser light $\lambda = 450\ nm$.

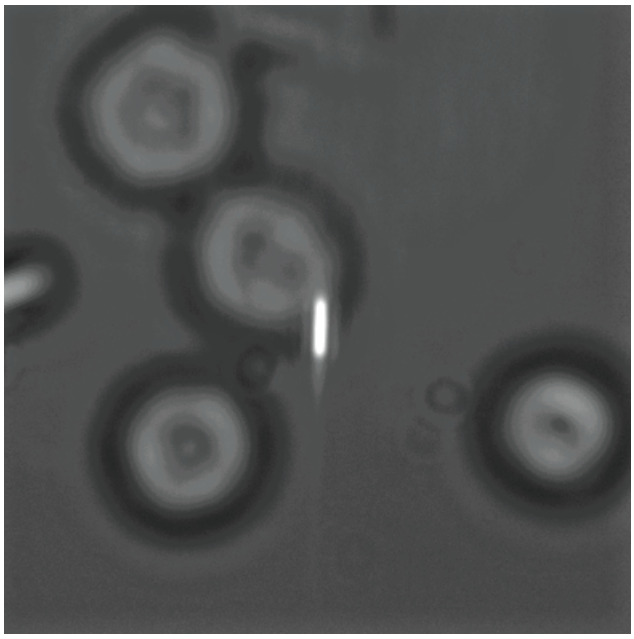

Figure 28: The laser spot focused on a sample holder with living cells. The spheres in the background are HEK-cells with a typical diameter of approximately 10 μm. Configuration of the setup: low laser intensity, objective lense with magnification of x40.

Re-calibration of laser safety: For safe operation of the setup the laser intensity coming out of the eyepiece should be on a tolerable low level. This can be achieved by simply turning one of the polarisation filters until the measured intensity is at a minimum.

6.3. Laser time/intensity profile

For better classification of the used laser light, the time/intensity profile of the laser light pulses has been investigated. For this purpose an optical power monitor and energy meter console (Thorlabs Instrumentation, PM100D) with a compact photo diode power head with silicon detector (Thorlabs Instrumentation, S121C, $400 - 1100\ nm$) has been used. This optical power monitor is able

to detect light intensities of single wavelengths on a $\approx 71\ mm^2$ circular area.

Figure 29 shows the measured profile while the digital signal (Arduino) was $\Delta t = 10\ ms$ on. The intensity rises over the course of $\Delta t = 9.2\ ms$ to a maximum power of $P = 1.1\ mW$.

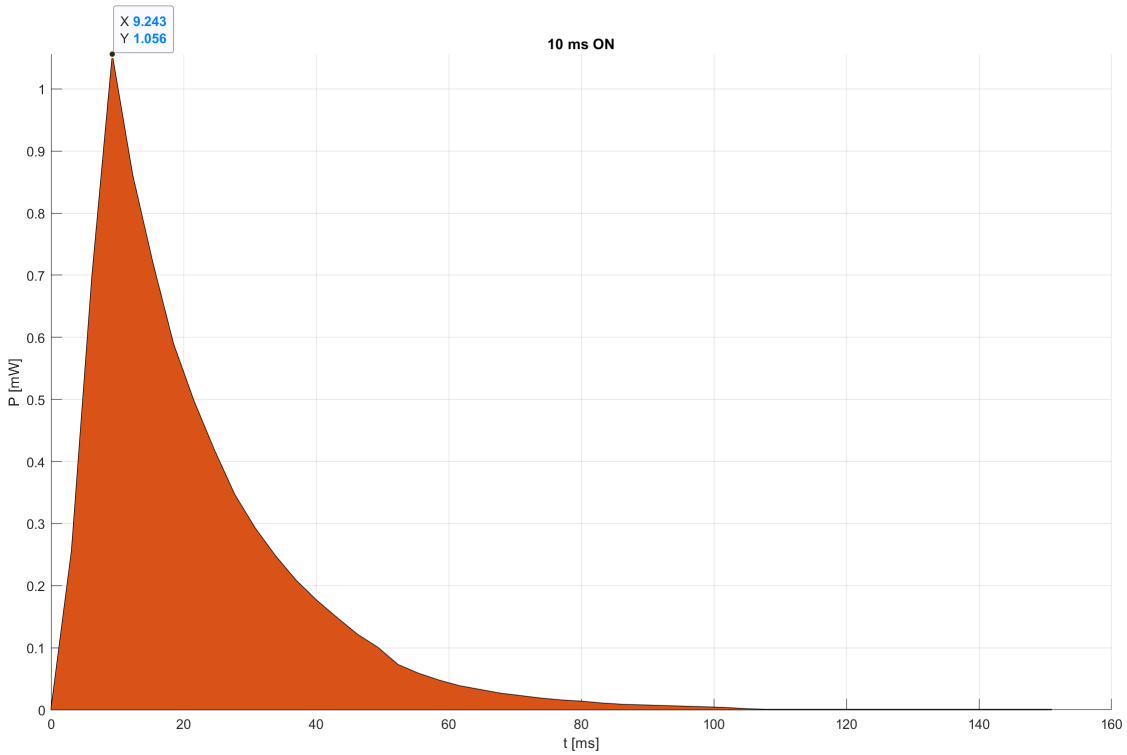

Figure 29: Optical intensity output profile of a $\Delta t = 10\ ms$ (digital ON time) laser pulse directly measured at the focus plane of the sample. Measured with a photo diode power head with silicon detector (Thorlabs Instrumentation, S121C, $400 - 1100\ nm$) directly in the focal plane of the sample holder.

The maximum intensity of the laser strongly depends on the pulse time (see figure 30). For a $\Delta t = 100\ ms$ pulse the output power is almost four times higher than for a $\Delta t = 10\ ms$ laser pulse.

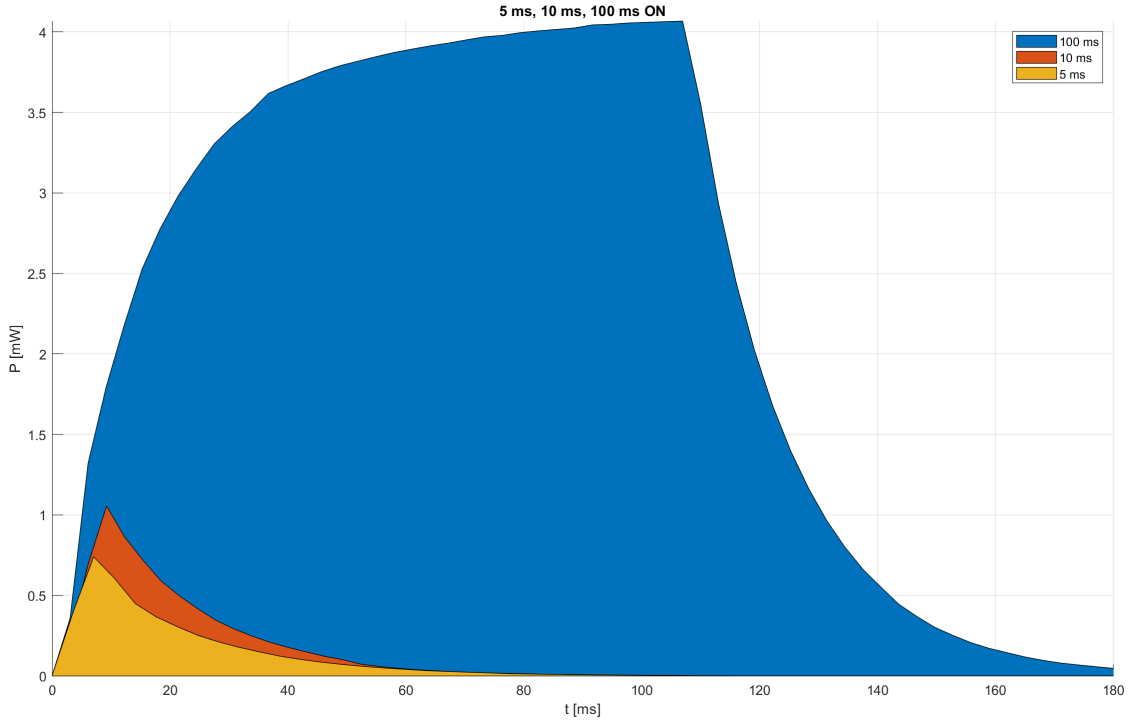

Figure 30: Optical output profiles of different ($\Delta t = 5,\ 10,\ 100\ ms$) laser pulses. Measured with a photo diode power head with silicon detector (Thorlabs Instrumentation, S121C, $400-1100\ nm$) directly in the focal plane of the sample holder.

A rough estimation gives us a feeling about the laser powers that occur. As example we use the laser pulse in fig 29:

The laser power P integrated over time gives us the total optical laser output energy E_{tot} of

$$P = \int_0^{\Delta t} P(t)\ dt = E_{tot} \approx 22\ mJ.$$

Under the assumption of a laser spot area of roughly $A_{spot} \approx 5\ \mu m^2$ this gives a laser power/energy per area of

$$\frac{P}{A_{spot}} = 0.2 \ \frac{mW}{\mu m^2}$$

$$\frac{E_{tot}}{A_{spot}} = 4.4 \ \frac{mJ}{\mu m^2}.$$

However, this value is higher for a $\Delta t = 100 \ ms$ pulse, where the laser power can be up to $^{P}/_{A_{spot}} = 1 \ ^{mW}/_{\mu m^2}$ in this configuration (this is in the mid range of the initial laser output power). Laser power intensities significantly higher than $1 \ ^{mW}/_{\mu m^2}$ are possible. The maximum was not measured as it was out of the detection range of the detector.

6.4. Patch clamp experiment

Figure 31 shows the first experiments conducted with the setup. The patch clamp pipette is docked with a HEK-cell in whole-cell configuration and the cell is connected to the epindolidione hedgehog structures. The laser was focused onto the semiconductor pigments before adjusting the patch clamp pipettes. While recording the electrophysiological behaviour of the cell with the patch clamp setup, the laser runs a program that turns the laser 10/50/100 ms on with pauses of 1000 ms. The results, depicted in figure 32, show a clear depolarisation of the HEK-cell membrane up to $\Delta V_M \approx 3.6 \ mV$ while the laser beam is active.

Control experiments have been conducted to further confirm the mechanism of laser induced cell membrane depolarisation with organic semiconductor structures by:

1.) Shooting the laser at cells without contact to the semiconductor structures.

2.) Shooting the laser at a semiconductor structure while placing the patch pipette near the pigment.

3.) Shooting the laser directly at the pipette without cells and semiconductor

structures.

None of these experiments show a significant change in the patch clamp recordings.

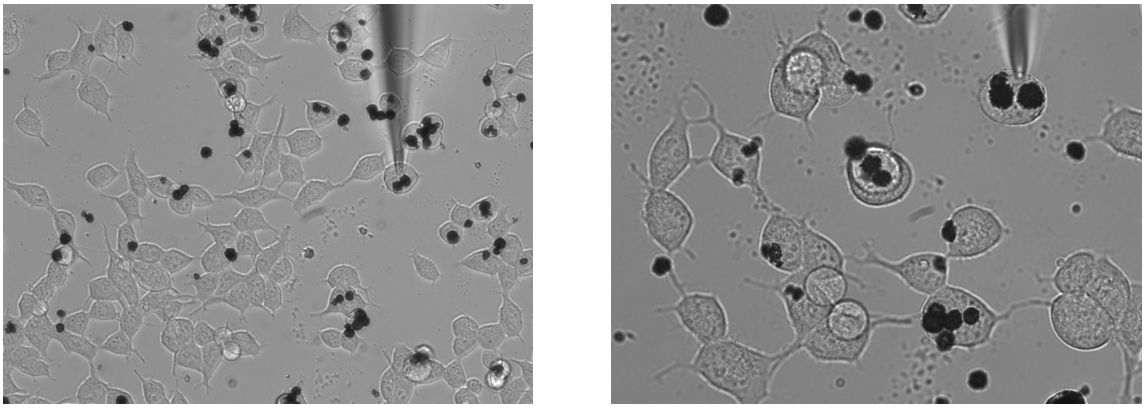

(a) (b)

Figure 31: Patch clamp experiment with epindolidione hedgehog structures and HEK-cells. The patch pipette is docked with the cell and the laser is focused (but turned off) on the semiconductor structure attached to the HEK-cell. (a) Magnification x20 (b) Magnification x40

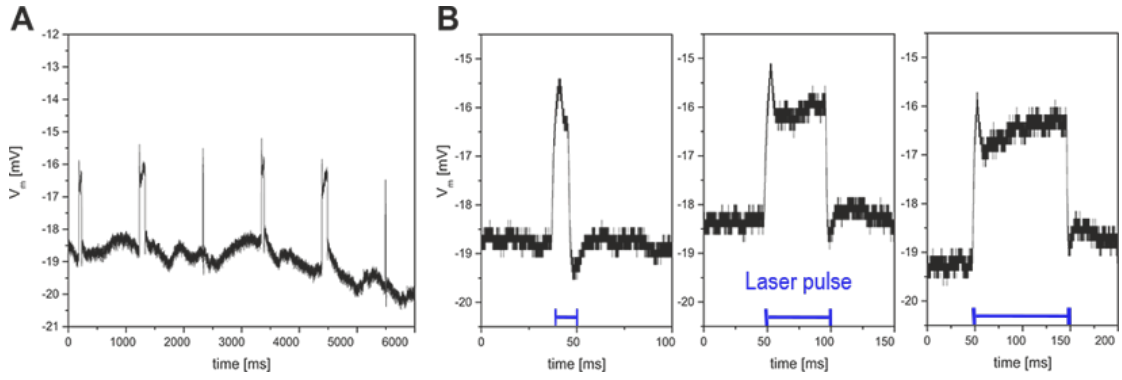

Figure 32: First proof of concept measurement. The membrane potential of the HEK-cells could be depolarised by focusing the laser directly onto the epindolidione hedgehog structures attached to the cells. The laser runs a program that turns the laser 10/50/100 ms on with pauses of 1000 ms.

The extracellular and intracellular solutions used for the patch clamp experiments can be seen in table 2 and table 3.

Table 2: Extracellular 2 mM Ca^{2+} solution used for the HEK-Cell patch clamp experiments. Water used is $ddH2_O$ (double distilled water) adjusted pH to 7.4 with $NaOH$.
c - concentration
Mw - molar weight
HPES - buffer

Compound	**c [mM]**	**Mw [g/mol]**
NaCl	140	58.44
KCl	5	74.55
$MgCl_2$	1	203.30
HEPES	10	238.30
Glucose	10	198.17
$CaCl_2$	2	147.02

Table 3: Intracellular K solution used for the HEK-Cell patch clamp experiments. Water used is ddH_2O (double distilled water) adjusted pH to 7.4 with KOH.
c - concentration
Mw - molar weight
HPES - buffer

Compound	**c [mM]**	**Mw [g/mol]**
KCl	5	74.55
$MgCl_2$	1	203.30
HEPES	10	238.30
Glucose	10	198.17

7. Discussion and outlook

Among the most important aspects in artificial cell stimulation are the physical concepts responsible for the plasma membrane depolarisation. Current literature has clearly decribed that this stimulation can be in fact traced back to a mixture of the capacitive effect, the faradaic effect and the thermocapacitive effect (see section 3.1.4). The big question concerning every technology in artificial cell stimulation is to which percentage the membrane depolarisation divides into this effects. The most favourable effect is the capacitive effect, as this is the most efficient and physiological effect. The least favourable effect is the faradaic effect as this phenomenon is likely to produce toxins (H_2O_2). The maximum temperature increase of the plasma cell membrane is limited, as too high temperatures can damage the cell. Therefore, the optimum device for light induced artificial cell membrane stimulation would be a bio compatible, photo capacitive device that is in the dimension of a single cell, exhibits no signs of faradaic effects and shows limited thermocapacitive effects. To efficiently stimulate a living cell this device needs suitable material properties such as a high quantum yield, a broad and efficient absorption coefficient (band gap for visible light) and a high charge carrier mobility.

Quinacridone nano hedgehog structures constitute a promising first attempt to use organic semiconductor pigments for artificial photo induced cell membrane stimulation. This technology is however suspected to mainly utilise the thermocapacitive effect for cell stimulation. Epindolidione structures as used in this thesis show a certain extent of H_2O_2 production [8]. As the light stimulation is within microseconds and individual epindolidione structures are in micrometer size, a direct evaluation of potentially generated H_2O_2 is technically not possible.

To benefit from photo capacitive depolarisation organic semiconductor pigments need to form a p-n junction in order to separate photo induced excitons [8] and therefore generate a potential difference. Epindolidione hedgehog structures represent the next step in this research as they show superior material properties compared to quinacridone nano structures. Future research will investigate epindolidione hetero structures forming a p-n junction caused by two different crystal phases. This is expected to add photo capacitive and increased faradaic depolarisation to the thermocapacitive effect and therefore improve the overall efficiency of artificial photo induced cell stimulation.

The mechanism of thermocapacitive depolarisation relies on the theory that the capacitance of the plasma cell membrane is a function of the temperature. Currently, researchers in the field use empirical values to describe the capacitance change of the cell membrane [14]. Further knowledge of the theoretical background could improve the understanding of this phenomenon. To get to the rather simple differential equation 12 various approximations were needed. One major approximation not mentioned in section 3 is the fact that the membrane resistance R_M of the cell membrane can not be considered constant. The membrane resistance decreases with temperature as the mobility of ions responsible for the current through the membrane is temperature dependent. The membrane resistance can be derived from the Arrhenius equation [10]:

$$ln(R_M(T(t)) = \frac{a}{T(t)} + c. \tag{24}$$

Here a and c are empirical parameters. Coupling the temperature dependence of the membrane resistance with the differential equation 12 could improve the

[8] Excitons are quantized quasi-particles which describe the bound state of electrons and electron holes.

theory behind the thermocapacitive effect.

To further increase the efficiency of photo induced cell membrane depolarisation a large and close interface with the cell to the stimulating object is beneficial. Electron microscopy imaging shows that epindolidione nano architectures can form close interfaces analogously to quinacridone (see section 4.5). Neurons apparently show the tendency to voluntarily advance their dendrites to the epindolidione pigments (see section 4.5 and 6.1). Other experiments within our research group show that the growing and moving embryonic neurons tend to incorporate the pigments (see figure 33). We suspect the large surface caused by the geometry of the hedgehog structure to be the root for the relatively strong electrostatic interface bondage of the soma and the dendritic branches. The strong bonding of the structures to the cell membrane might be one of the key features for the applicability of this technology.

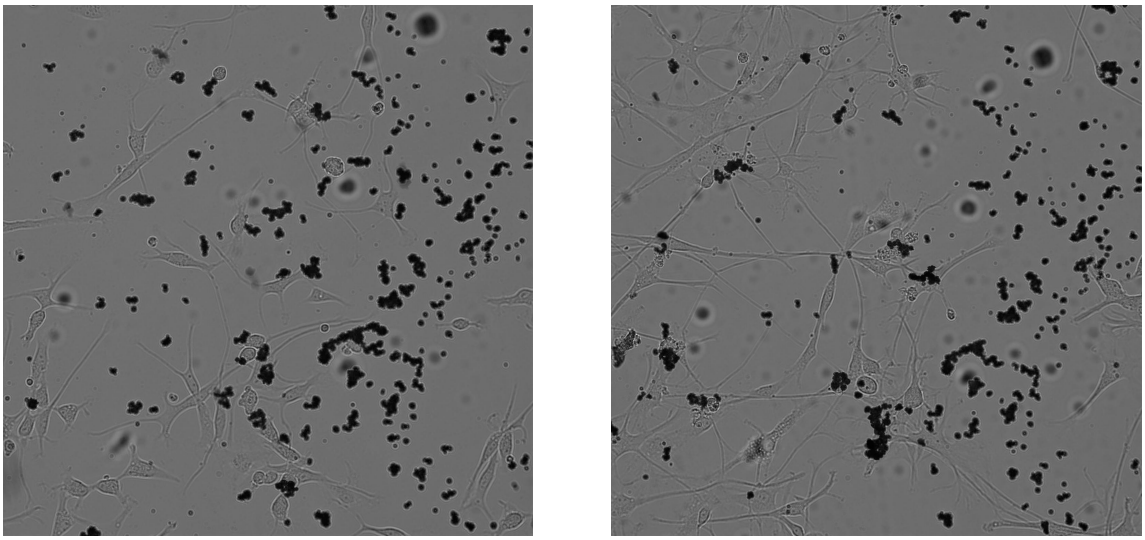

(a) (b)

Figure 33: Embryonic rat cortex neurons growing over course of 72h on a sample with epindolidione hedgehog structures. The images are form the same video: (a) $t = 0\ h$, neurons start to grow and interacting with the epindolidione pigments. (b) $t \approx 72\ h$, the neurons collect the structures and bundle them near the soma.

In order to depolarise the plasma membrane of the cells connected to the pigments I chose to focus a 450 nm laser onto the semiconductor strictures. The reason this laser wavelength was chosen is simply the broad availability of cheap 450 nm laser pointers as well as the smaller peak in the absorption coefficient of H-bonded epindolidione at $\approx$ 455 nm (see figure 12). The absorption of a laser with 490 nm would be more than two times higher than at 450 nm wavelength. However, the modular design of the setup ensures easy switching of the laser beam source to increase the efficiency of measuring with epindolidione and other materials.

As we learned from relation 22 the energy E_{Th} needed for triggering action potentials in excitable cells decreases with the square root of the pulse duration Δt of the incident laser (see section 3.3). In this setup the pulse duration is regulated via turning the laser on and off using a digital signal and a relay. From figure 30 we see that the laser intensity increases over the course of the digital on signal and then decreases exponentially when the laser is turned off. Amongst other things this might be due to the slow reaction time of the solid state laser. In fact this can be utilised to regulate the intensity of the pulse, but it can be barely used to shorten the pulse time. With this configuration the relatively short pulse times needed for optimal cell stimulation can not be reached.

To solve this problem it would be feasible to chop the laser light into defined pulses using an acousto-optic modulator (AOM) while running the laser continuously. This would cause a laser pulse that increases and decreases faster, i.e. the laser gets chopped into a signal that gets closer to a square wave and therefore would be more suitable for heating up the semiconductor structures. Currently a variation in operation voltage is used to control the output intensity of the laser light. This works because the output intensity of a solid state laser is generally a linear function of the operating voltage. However, this function can differ in the edge region. To ensure constant and reproducible laser light

intensities the characteristic line of the laser should be measured. A more stable solution would be to run the laser at a constant intensity while adjusting the laser light intensity with filters of different optical density. This filters however need to be placed by hand in the optical path.

The first experiments with this setup exhibit a distinct but too small depolarisation of HEK-cell plasma membrane. To clearly show the mechanism of photo induced cell stimulation with organic semiconductor structures further experiments with an improved experimental setup should be conducted. The ultimate aim of this experimental setup would be to proof that the generation of action potentials in excitable cells in contact with organic semiconductor structures through laser induced cell membrane depolarisation is feasible.

8. Summary

For better understanding of photo induced cell stimulation with organic semiconductor structures the theoretical principle of the thermocapacitive effect on a cell membrane has been investigated (see section 3). The energy E_{Th} needed for triggering action potentials in excitable cells decreases with the square root of the pulse duration Δt of the incident laser (see section 3.3)

The organic semiconductor tetracene and its H-bonded crystal epindolidione shows superior material properties to tetracene and its H-bonded crystal quinacridone in respect of photo induced cell membrane stimulation (see sections 4.1-4.2).

The interface between epindolidione nano architectures and neurons has been investigated with electron microscopy imaging (see section 4.4).

A Matlab routine has been written to quantitatively analyse embryonic neuronal interaction with organic semiconductor structures over time (see section 6.1).

An experimental setup has been built to survey the mechanism of photo induced cell stimulation with organic semiconductor structures (see section 5). The setup uses a 450 nm laser coupled into the back of an inverted microscope while making electrophysiological (patch-clamp) recordings feasible. The first experiments exhibit a small but significant depolarisation of HEK-cell plasma membrane (see section 6).

List of Equations

List of Figures

List of Tables

References

[1] Laser safty. https://www.osha.gov/dts/osta/otm/otm_iii/otm_iii_6.html#4. Accessed: 12.08.2019.

[2] Wolfhard Almers. Gating currents and charge movements in excitable membranes. In *Reviews of Physiology, Biochemistry and Pharmacology, Volume 82*, pages 96–190. Springer, 1978.

[3] Joao L Carvalho-de Souza, Bernardo I Pinto, David R Pepperberg, and Francisco Bezanilla. Optocapacitive generation of action potentials by microsecond laser pulses of nanojoule energy. *Biophysical journal*, 114(2):283–288, 2018.

[4] João L Carvalho-de Souza, Jeremy S Treger, Bobo Dang, Stephen BH Kent, David R Pepperberg, and Francisco Bezanilla. Photosensitivity of neurons enabled by cell-targeted gold nanoparticles. *Neuron*, 86(1):207–217, 2015.

[5] Kenneth S Cole. *Membranes, ions and impulses: a chapter of classical biophysics*, volume 1. Univ of California Press, 1972.

[6] Agamemnon Despopoulos and Stefan Silbernagl. *Color atlas of physiology*. Thieme, 2003.

[7] Eric Daniel Głowacki, Mihai Irimia-Vladu, Martin Kaltenbrunner, Jacek Gsiorowski, Matthew S White, Uwe Monkowius, Giuseppe Romanazzi, Gian Paolo Suranna, Piero Mastrorilli, Tsuyoshi Sekitani, et al. Hydrogen-bonded semiconducting pigments for air-stable field-effect transistors. *Advanced Materials*, 25(11):1563–1569, 2013.

[8] Maciej Gryszel, Mykhailo Sytnyk, Marie Jakesova, Giuseppe Romanazzi, Roger Gabrielsson, Wolfgang HeiSS, and Eric Daniel Glowacki. General Observation of Photocatalytic Oxygen Reduction to Hydrogen Peroxide by Organic Semiconductor Thin Films and Colloidal Crystals. *ACS Applied Materials and Interfaces*, 10:13253–13257, 2018.

[9] Bertil Hille. *Ionic channels in excitable membranes.*, volume 2. Elsevier, 1978.

[10] Yuanwen Jiang, Ramya Parameswaran, Xiaojian Li, João L Carvalho-de Souza, Xiang Gao, Lingyuan Meng, Francisco Bezanilla, Gordon MG Shepherd, and Bozhi Tian. Nongenetic optical neuromodulation with silicon-based materials. *Nature protocols*, 14(5):1339, 2019.

[11] William J Krause. *Krause's essential human histology for medical students.* Universal-Publishers, 2005.

[12] Armstrong JD Longair MH, Baker DA. Simple neurite tracer. Bioinformatics, 2011.

[13] Ingmar Schön. *Extrazelluläre Stimulation von Ionenkanälen und Nervenzellen mittels Elektrolyt/Oxid/Silizium-Kondensatoren.* PhD thesis, Technische Universität München, 2006.

[14] Mikhail G Shapiro, Kazuaki Homma, Sebastian Villarreal, Claus-Peter Richter, and Francisco Bezanilla. Infrared light excites cells by changing their electrical capacitance. *Nature communications*, 3:736, 2012.

[15] Mykhailo Sytnyk, Marie Jakešová, Monika Litviňuková, Oleksandr Mashkov, Dominik Kriegner, Julian Stangl, Jana Nebesářová, Frank W Fecher, Wolfgang Schöfberger, Niyazi Serdar Sariciftci, et al. Cellular interfaces with hydrogen-bonded organic semiconductor hierarchical nanocrystals. *Nature communications*, 8(1):91, 2017.

[16] Robert E Taylor. Impedance of the squid axon membrane. *Journal of Cellular and Comparative Physiology*, 66(S2):21–25, 1965.

[17] Wolfgang Tress. Organic solar cells. In *Organic Solar Cells*, pages 67–214. Springer, 2014.

[18] Bilz0r (Wikipedia). Image of the four patch-clamp modes. Wikipedia, 2008. public domain: https://commons.wikimedia.org/wiki/File:Patchmodes.svg; date: 19. July 2019.

[19] Chris 73 (Wikipedia). Schematic of an action potential. Wikipedia, 2007. creative commons: https://commons.wikimedia.org/wiki/File:Action_potential.svg; date: 19. July 2019.

[20] PeaBrainC (Wikipedia). Patch clamp schematic 2. Wikipedia, 2018. public domain: https://commons.wikimedia.org/wiki/File:Patch_clamp_schematic_2.png; date: 19. July 2019.

[21] Synaptidude (Wikipedia). Basis of membrane potential2. Wikipedia, 2011. creative commons: https://commons.wikimedia.org/wiki/File:Basis_of_Membrane_Potential2.png; date: 15. July 2019.

,

Appendices

A. Matlab code for statistical evaluation of neuronal growth

```
clear all
close all
clc
tic

%% collecting data

path_1 = 'C:\Users\stili\Dropbox\Masterarbeit Clemens\
    Neuron tracing\Neuron Tracing neu';
     % Neuron 4 did not work
     % Neuron 12 is the example neuron
     % Umrechnungsfaktor zwischen pixel und micrometer:
        pixel*0.625 = micrometer (alte cellobservervideos)


Name = ['Neuron ', path_1(end-1:end)]

addpath(genpath(path_1))

data_a = dir([path_1, '/*.swc']);
data_num = size(data_a,1)

if true
     matfiles = dir(fullfile([path_1,'\*.swc']));
```

```
23
24      M  = cell(150,1);
25
26      n= data_num; % Enter number of pictures plus empty
            pictures (standad = 141)
27
28      n0= 1; % Enter starting number of first picture (n0=
            141 - #data +1)
29
30
31
32      for i= n0:n
33
34          M{i}= importdata(matfiles(i-n0+1).name);
35          S{i}= M{i}.data;
36          x{i}= S{i}(1:end,3);
37          y{i}= S{i}(1:end,4);
38
39      end
40
41  end
42
43
44  %% Länge der Dentriten berechnen
45
46  for i= 1:n
47
48      L{i}= sum(sqrt(diff(x{i}).^2 + diff(y{i}).^2));
49      L_S(i)= sum(L{i});
50
```

```
51 end
52
53
54
55 %% Dynamik des Dentriten (Standardabweichung)
56
57 mu= sum(L_S)/n;
58
59 d1 = ['Mean Length of Dentrit = ',num2str(mu),' [pixel] '
       ];
60 disp(d1)
61
62
63
64
65 for i= 1:n
66
67     sigma= sqrt( ((L{i}-mu)^2)./n );
68
69 end
70
71
72 d2 = ['Dynamik of Dentrit (standard deviation) = ',
      num2str(sigma),' [pixel] '];
73 disp(d2)
74
75
76
77 %% plot all traces
78
```

```
79 h1 = figure
80
81 for i= n0:n
82
83     hold on
84
85     plot(x{i},y{i})
86     plot(x{i}(1),y{i}(1),'*')
87     plot(x{i}(end),y{i}(end),'o')
88
89 end
90
91 grid on
92 title('growth of dendtrit, * - Start, O - Ende')
93 xlabel('x [pixel]')
94 ylabel('y [pixel]')
95 hold off
96
97 %% plot dentrit length over time
98
99 h2 = figure
100
101 t= linspace(1,73,n);
102
103
104
105 plot(t,L_S)
106
107 title('dentrit length over time')
108 xlabel('t [h]')
```

```
109 ylabel('l [pixel]')
110 grid on
111 hold off
112
113 v = L_S ./ t;
114
115
116
117 %% dynamic of ending points of dentrit
118
119
120 for i= n0:n
121
122     x_e(i)= x{i}(end);
123     y_e(i)= y{i}(end);
124
125 end
126
127 k = find(x_e);
128
129 l_ex = x_e == 0;
130
131 x_e(l_ex) = x_e(k(1));
132
133
134 p = find(y_e);
135
136 l_ey = y_e == 0;
137
138 y_e(l_ey) = y_e(p(1));
```

```
139
140
141 h3 = figure
142 hold on
143 z = zeros(size(x_e));
144 col = t;  % This is the color, vary with x in this case.
145 surface([x_e;x_e],[y_e;y_e],[z;z],[col;col],...
146     'facecol','no',...
147     'edgecol','interp',...
148     'linew',2);
149 title('progression of dentrit endpoint by time')
150 c = colorbar;
151 c.Label.String = 't, Time [h]';
152 xlabel('x [pixel]')
153 ylabel('y [pixel]')
154 plot(x_e,y_e,'o')
155 grid on
156 hold off
157
158 %% endpoint dynamic
159
160
161 L_e= sqrt(diff(x_e).^2 + diff(y_e).^2);
162
163 L_e(end+1)= 0;
164
165
166 h4 = figure
167 hold on
168
```

```
169 plot(t,L_e,'-.')
170 plot(t,L_e,'or')
171
172
173 title('dynamic of dentrit endpoint by time')
174 xlabel('x [pixel]')
175 ylabel('y [pixel]')
176 grid on
177
178 saveas(h1,[Name,' start end'],'png');
179 saveas(h2,[Name,' length over time'],'png');
180 saveas(h3,[Name,' progression of endpoint'],'png');
181 saveas(h4,[Name,' dynamic of endpoint'],'png');
182
183 % saveas(h1,Name,'png');
184
185 toc
```

B. Used code for laser controlling

```
1
2         // include the library code:
3 #include <LiquidCrystal.h>
4
5 // initialize the library by associating any needed LCD interface
    pin
6 // with the arduino pin number it is connected to
7 const int rs = 52, en = 50, d4 = 48, d5 = 46, d6 = 44, d7 = 42;
8 LiquidCrystal lcd(rs, en, d4, d5, d6, d7);
9
10
11
12
13 //rotary
14
15 #define outputA 3
16 #define outputB 4
17
18 int counter = 0;
19 int aState;
20 int aLastState;
21 const int rotbutt = 2;
22 int Delay;
23
24
25
26 //Polyc.
27
28 int anglePin = 9;
29 int shutterPin = 34;
30 int value = 0;
31 float k = 0.8058;
32 int u = 0;
33 int lambda = 0;
```

```
34 int mode = 0;
35 int rot;
36 int buttonState;
37 int lastButtonState;
38 int buttonPushCounter;
39 int poti = A0;
40 int a1;
41 int SW = 8;
42
43
44
45
46 void setup() {
47   lcd.begin(16, 2);
48   pinMode(anglePin, OUTPUT);
49   pinMode(shutterPin, OUTPUT);
50   pinMode(poti, OUTPUT);
51   pinMode(A1, INPUT);
52
53   pinMode(rotbutt, INPUT);
54   pinMode(outputA, INPUT);
55   pinMode(outputB, INPUT);
56
57   pinMode(SW, OUTPUT);
58
59   Serial.begin (9600);
60   aLastState = digitalRead(outputA);
61 }
62
63
64
65 void loop() {
66   value = 186.15; // 0V-3.65V is 0-186.15 is 300nm-450nm
67
68   lambda = 0;
69
```

```
70  digitalWrite(shutterPin, HIGH);
71
72
73  digitalWrite(SW, HIGH);
74  delay(7000);
75  digitalWrite(SW, LOW);
76  delay(7000);
77
78
79
80  //  delay(100);
81  //  analogWrite( shutterPin, 85);
82  //  delay(100);
83  //  analogWrite( shutterPin, 150);
84
85
86    analogWrite(anglePin, u);
87
88    rot = digitalRead(rotbutt);
89
90
91
92    aState = digitalRead(outputA);
93
94    if (aState != aLastState) {
95      if (digitalRead(outputB) != aState) {
96        counter++;
97      }
98      if (digitalRead(outputB) >= aState) {
99        counter--;
100     }
101     if (counter > 30) {
102       lcd.clear();
103       counter = 1;
104     }
105     if (counter < 0) {
```

```
106         lcd.clear();
107         counter = 29;
108       }
109       Serial.print("Position: ");
110       Serial.println(counter);
111     }
112     aLastState = aState;
113
114
115
116     buttonState = digitalRead(rotbutt);
117
118     // compare the buttonState to its previous state
119     if (buttonState != lastButtonState) {
120       // if the state has changed, increment the counter
121       if (buttonState == HIGH) {
122         // if the current state is HIGH then the button went from off
                to on:
123         buttonPushCounter++;
124         if (buttonPushCounter > 6)
125           buttonPushCounter = 1;
126         Serial.print("number of button pushes: ");
127         Serial.println(buttonPushCounter);
128         lcd.setCursor(14, 0);
129         lcd.print("WL");
130       }
131     }
132     lastButtonState = buttonState;
133
134
135
136
137
138     lambda = lambda + counter * 5 + 300;
139
140     if (buttonPushCounter == 1) {
```

```
141       analogWrite(poti,255);
142       a1 = analogRead(A1);
143   //     Serial.println(a1); if someone reads this I owe you a beer
144
145       lcd.setCursor(0, 0);
146       lcd.print("WL= ");
147
148       lcd.setCursor(4, 0);
149       lcd.print(lambda);
150
151       u = (lambda - 300) / k;
152       analogWrite(anglePin, u);
153
154       lcd.setCursor(7, 0);
155       lcd.print(" nm");
156     }
157
158
159     if (buttonPushCounter == 2) {
160       lambda = 340;
161       Delay = 100;
162       u = (lambda - 300) / k;
163
164       lcd.setCursor(0, 0);
165       lcd.print("WL= ");
166
167       lcd.setCursor(14, 0);
168       lcd.print("SW");
169
170       lcd.setCursor(4, 0);
171       lcd.print(lambda);
172
173       lcd.setCursor(7, 0);
174       lcd.print(" nm");
175
176       lcd.setCursor(9, 1);
```

```
177       lcd.print(Delay);
178       lcd.setCursor(14, 1);
179       lcd.print("ms");
180     }
181     else {
182     }
183
184
185     if (buttonPushCounter >= 3) {
186       lcd.setCursor(0, 0);
187       lcd.print("WL= ");
188
189       lcd.setCursor(14, 0);
190       lcd.print("FS");
191
192       lcd.setCursor(4, 0);
193       lcd.print("340/380nm");
194
195       if (buttonPushCounter == 4) {
196
197         Delay = 100 + 50 * counter;
198         if (Delay >= 1001) {
199           Delay = 100;
200           counter = 1;
201           lcd.clear();
202         }
203         lcd.setCursor(0, 0);
204         lcd.print("WL= ");
205         lcd.setCursor(14, 0);
206         lcd.print("FS");
207
208         lcd.setCursor(4, 0);
209         lcd.print("340/380nm");
210
211         lcd.setCursor(10, 1);
212         lcd.print(Delay);
```

```
213         lcd.setCursor(14, 1);
214         lcd.print("ms");
215         lcd.setCursor(0, 1);
216         lcd.print("select:");
217       }
218
219       if (buttonPushCounter == 5) {
220         lambda = 340;
221         lcd.setCursor(0, 0);
222         lcd.print("WL= ");
223         u = (lambda - 300) / k;
224         analogWrite(anglePin, u);
225
226         lcd.setCursor(14, 0);
227         lcd.print("FS");
228
229         lcd.setCursor(4, 0);
230         lcd.print("340/380nm");
231         lcd.setCursor(10, 1);
232         lcd.print(Delay);
233         lcd.setCursor(14, 1);
234         lcd.print("ms");
235
236         delay(Delay);
237
238         lambda = 380;
239         lcd.setCursor(14, 0);
240         lcd.print("  ");
241         lcd.setCursor(10, 1);
242         lcd.print("    ");
243         lcd.setCursor(14, 1);
244         lcd.print("  ");
245         u = (lambda - 300) / k;
246         analogWrite(anglePin, u);
247         delay(Delay);
248       }
```

```
249
250       if (buttonPushCounter == 6) {
251         lcd.clear();
252         buttonPushCounter = 1;
253       }
254     }
255   }
```